Formation and chemical evolution of SOA in two different environments: A dual chamber study

Andreas Aktypis[1,2], Dontavious J. Sippial[3], Christina N. Vasilakopoulou[1,2], Angeliki Matrali[1,2], Christos Kaltsonoudis[2], Andrea Simonati[1,2], Marco Paglione[4], Matteo Rinaldi[4], Stefano Decesari[4] and Spyros N. Pandis[1,2]

[1]Department of Chemical Engineering, University of Patras, Patras, Greece
[2]Institute of Chemical Engineering Sciences (ICE-HT), FORTH, Patras, Greece
[3]Department of Chemical Engineering, Carnegie Mellon University, Pittsburgh, USA
[4]Italian National Research Council, Institute of Atmospheric Sciences and Climate (CNR-ISAC), Bologna 40129, Italy

10   *Correspondence to*: S. N. Pandis (spyros@chemeng.upatras.gr)

Abstract. A dual chamber system was deployed in two different environments to study the potential of ambient air, that was directly injected into the chambers, to form secondary organic and inorganic aerosol. A total of 16 experiments took place during March 2022 in a polluted environment in the Po Valley, Italy which is dominated by anthropogenic emissions. Another 15 experiments were conducted in the Pertouli forest, Greece which is dominated by biogenic emissions. In both campaigns,

15   ambient air containing highly oxidized (average O:C 0.7-0.8) aerosol was the starting point of the experiments and its chemical evolution under the presence of OH radicals was followed. In the Po Valley SOA formation was observed in all experiments but one and the formed SOA ranged from 0.1 to 10 μg m^{-3}. Experiments conducted under more polluted conditions (usually at night and early morning) had significantly higher SOA formation, with the concentration of the organic aerosol at the end being about four times higher than the initial. Also, production of 4-230 μg m^{-3} of ammonium nitrate was observed in all

20   experiments due to the high levels of ammonia in this area. The produced SOA increased as the ambient relative humidity increased, but there was not a clear relationship between the SOA and temperature. Higher SOA production was observed when the PM$_1$ levels in Po Valley were high. Contrary to the Po Valley, only one experiment in the Pertouli forest resulted in the formation of detectable SOA (about 1 μg m^{-3}). This experiment was characterized by higher ambient concentrations of both monoterpenes and isoprene. In two experiments, some SOA was formed, but its concentration dropped below detection

25   levels after 30 min. This behavior is consistent with local formation in a chamber that was not well mixed. Although both environments have OA with O:C in the range of 0.7-0.8, the atmosphere of the two sites had very different potentials of forming SOA. In the Po Valley, the system reacts rapidly forming large amounts of SOA, while in Pertouli the corresponding SOA formation chemistry appears to have been practically terminated before the beginning of most experiments, so there is little additional SOA formation potential left.

1 Introduction

About 300,000 premature deaths are estimated to occur annually in Europe due to air pollution, the vast majority (77%) of which are related to chronic exposure to fine particulate matter (EEA, 2023). Atmospheric aerosol has been widely connected to various diseases, especially of the cardiovascular and the respiratory systems but also the brain (Pope and Dockery, 2006). These particles are also responsible for the reduction of the atmosphere's visibility, while they play a key role in the climate system (Seinfeld and Pandis, 2016). Although the impacts of atmospheric aerosols on both climate and human health have been widely studied, large uncertainty remains about their chemical evolution in the atmosphere because their sources, composition, properties, and toxicity can vary dramatically from one environment to another.

Organic material accounts for 20-60% of the total fine aerosol mass on a global scale, and it can even reach 90% in tropical forests (Kanakidou et al., 2005). Due to its high availability and characteristics, it plays a predominant role in various physicochemical processes in the atmosphere. These include the formation of new particles and their subsequent growth (Kulmala et al., 2004; Kerminen et al., 2018), affecting climate both directly and indirectly (Seinfeld and Pandis, 2016), atmospheric aging, etc. Organic aerosol (OA) can be introduced in the atmosphere either directly (primary organic aerosol or POA) or can be formed through the oxidation of various organic vapors (secondary organic aerosol or SOA). The sources of POA include combustion processes, like biomass burning (wildfires, domestic heating etc.), transportation and cooking. A higher complexity characterizes the formation of SOA, which accounts for up to 90% of the total OA in both urban and rural environments (Huang et al., 2014; Chaturvedi et al., 2023). The gaseous precursors involved in SOA production originate from both biogenic and anthropogenic sources, interact with each other and the particle phase, and have different contributions to the formed SOA. The mechanisms and kinetics of SOA formation depend on ambient conditions, NO_x availability, preexisting OA, the oxidant (OH, O_3 or NO_3) involved, etc. (Kroll and Seinfeld, 2008).

The levels of SOA observed in the atmosphere are often underpredicted by chemical transport models as a result of our lack of understanding of the corresponding SOA formation pathways (Kanakidou et al., 2005; Volkamer et al., 2006; Robinson et al., 2007; Kroll and Seinfeld, 2008; Jimenez et al., 2009; Tsigaridis et al., 2014). While developments, such as the volatility basis set (Donahue et al., 2011) and accounting for the intermediate volatility organic compounds (IVOCs), have significantly improved model predictions, the problem of underestimation often persists. For example, heterogeneous reactions that may affect SOA formation are not fully incorporated even in most recent models (Jo et al., 2024). Another reason for this underprediction is that models rely on measurements obtained from laboratory chamber experiments, that typically test the potential of individual VOCs to form SOA (Kroll and Seinfeld, 2008). Although these laboratory experiments provide valuable insights about the chemical pathways the carbon of a specific VOC follows during and after its oxidation, they are not always able to explain ambient observations. For instance, the SOA formed in the ambient is usually far more oxidized than the one formed in atmospheric simulation chambers (Kroll and Seinfeld, 2008).

Biogenic volatile organic compounds (bVOCs) include isoprene (C_5H_8), monoterpenes ($C_{10}H_{16}$) and sesquiterpenes ($C_{15}H_{24}$) and are emitted at a higher rate on a global scale than their anthropogenic counterparts (Guenther et al., 2012; Seinfeld

and Pandis, 2016). Numerous laboratory studies have investigated the oxidation of these compounds (mainly isoprene and monoterpenes) by the hydroxyl radical (OH) ozone (O_3), and the nitrate radical (NO_3) (Griffin et al., 1999b; Kroll et al., 2006;

65 Qi et al., 2012; Müller et al., 2012; Wang et al., 2018a). Most of these efforts have focused on the first generation of reactions and the corresponding formation of SOA. The first-generation products, depending on their volatility and structure, can be further oxidized and produce later generations of products, a process known as chemical aging. Ng et al. (2006) suggested that several compounds containing double bonds, like many terpenes, continue to make a notable contribution to SOA formation even after undergoing their initial oxidation step. Donahue et al. (2012) analyzing data obtained from the Multiple Chamber

70 Aerosol Chemical Aging Study (MUCHACHAS) reported that OH aging of biogenic OA can notably enhance SOA concentrations due to the formation of later-generation products. The role of larger molecules like sesquiterpenes has also been investigated in a number of studies. These compounds have a high SOA formation potential (Griffin et al., 1999a; Barreira et al., 2021) and their later generation products can also contribute to the total SOA. Tasoglou and Pandis (2015) explored the chemical aging of β-caryophyllene and found that the products of its ozonolysis were able to form an additional 13-17% of

75 SOA mass, with the addition of OH radicals under high NO_x and low RH. Interestingly, under high RH (90%) the SOA mass increased by 40%. Studying the SOA formed from all these later generation reactions could be the key to connecting chamber studies and field measurements.

In urban, suburban and rural environments, where most people live, anthropogenic VOCs can actively participate in SOA formation, interacting with other anthropogenic and biogenic pollutants (He et al., 2021; Nault et al., 2021; Chaturvedi

80 et al., 2023). A recent toxicological study (Ito et al., 2019) suggested that SOA associated with anthropogenic sources led to elevated oxidative stress and inflammation in cells compared to biogenic SOA. Semi (C* between 1 and 100 μg m^{-3}) and intermediate (C* between 10^3 and 10^6 μg m^{-3}) volatility organic compounds (SVOCs and IVOCs, respectively) have been found to play a key role in the formation of SOA, despite their relatively lower ambient concentrations compared to other VOCs. Laboratory experiments have shown that these compounds have much higher SOA yields than the smaller VOCs (Chan

85 et al., 2009; Lim and Ziemann, 2009; Presto et al., 2010; Tkacik et al., 2012; Docherty et al., 2021). However, due to the experimental difficulties in measuring IVOC concentrations, there is still uncertainty about their exact role in SOA formation. Zhao et al. (2014) estimated that IVOCs were responsible for 30% of the SOA formed during afternoon hours in an urban environment in the US.

Even if investigations of the chemical evolution of specific VOCs and IVOCs within controlled chambers provides

90 valuable information about their potential to form SOA, the corresponding experimental conditions frequently deviate from real-world atmospheric conditions. The use of ambient air as a starting point in chamber experiments can help connect ambient observations with laboratory experiments. Kaltsonoudis et al. (2019) designed a dual chamber system to perform such experiments. Jorga et al. (2021) utilized this system to explore the nighttime chemistry of biomass burning emissions in an urban area in Greece. The system enabled them to quantify the rather high potential of the actual ambient air to form SOA

95 even during periods with low photochemistry. The portability of the system and its easy setup makes it useful in challenging environments, such as forests. In this study, we take advantage of the highly aged aerosol in two different environments (one

polluted and one more pristine inside a forest), to investigate their potential to form additional SOA, through oxidation of the existing VOCs, IVOCs and SVOCs. We focus on oxidation by OH radicals at different NO_x conditions. The dual chamber system was initially deployed at a rural site in the Po Valley, Italy, an area that is highly polluted and dominated by

100 anthropogenic emissions. The same system was also deployed, in Pertouli, a remote Greek forest, that is expected to be dominated by biogenic emissions. The only commonality about these two sites was the nearly identical (and relatively constant) ambient OA oxygen-to-carbon ratio (O:C) indicating highly aged aerosols in both environments. The results of all the conducted experiments are synthesized to provide insights into the SOA formation potential of the two different environments.

2 Methods

105 ### 2.1 Sites and field campaigns description

2.1.1 FAIRARI campaign

The Fog and Aerosol InteRAction Research Italy (FAIRARI) field campaign (November 2021 - May 2022) was conducted at San Pietro Capofiume (SPC), a rural site in the southern part of the Po Valley in Northern Italy (Fig. S1). The main objectives of the campaign were the investigation of the interactions between aerosol and fog, the formation and chemical evolution of

110 SOA and the driving mechanisms of new particle formation in a polluted atmosphere. Details about the campaign can be found in the overview paper by Neuberger et al. (2024).

The greater Po Valley area is one of the most polluted environments in Europe (Decesari et al., 2014; Daellenbach et al., 2020; EEA, 2023). Due to its high population density, orography, and the intense industrial and agricultural activities it is dominated by anthropogenic sources (Decesari et al., 2014). During the cold period (winter and early spring) the introduction

115 of biomass burning emissions in the atmosphere exacerbates the already poor air quality. Paglione et al. (2020) reported that SOA dominates OA, contributing at any given moment more than 65% of the OA, with an annual average of 83 ±16 %. The ambient OA O:C is of the order of 0.7-0.9 implying indeed aged aerosol (Paglione et al., 2020). During the cold period, the high liquid aerosol water content has also been found to participate in the ageing process. The conditions in this region during the cold period (elevated concentrations of NO_x, NH_3, low temperature, high humidity) create an ideal environment for the

120 formation of secondary inorganic aerosol (Squizzato et al., 2013). High efficiency in the formation of ammonium nitrate in SPC during this period has been reported (Paglione et al., 2021).

A total of 16 experiments (including 2 blanks, in which there was no OH production) were conducted during the FAIRARI campaign, between 2 and 17 March, 2022 (Table 1).

2.1.2 SPRUCE-22 campaign

125 The Summer PeRtoUli Campaign Emissions (SPRUCE-22) field campaign was conducted during July 2022, in Pertouli, a remote mountainous forested site in Greece (Fig. S1). Its main objective was to quantify the interactions between pollutants

transported over long distances and biogenic emissions in the Eastern Mediterranean. It combined both chamber experiments and ambient measurements (Vasilakopoulou et al., 2023; Matrali et al., 2024). Situated at an elevation of 1300 meters above sea level, the site was positioned at the chalet atop the Pertouli ski resort (39° 32'44"N 21° 29'55"E), in the middle of a spruce-fir forest. More information about the campaign can be found in Matrali et al. (2024).

The area is characterized by high biogenic emissions, especially of isoprene and monoterpenes (Harrison et al., 2001). Due to fast photochemistry during the summer, these are rapidly oxidized resulting in relatively low ambient concentrations. PMF analysis revealed that the biogenic oxidized factor accounted for 23% of the total, the rest being less-oxidized OA (37%) and more-oxidized OA (40%) (Vasilakopoulou et al., 2023). Detailed analysis of the latter suggested that it was mostly a result of rapid chemical aging and transport of wildfire emissions, originating hundreds of kilometres away from the site (Vasilakopoulou et al., 2023). However, biogenic SOA was also present in the less-oxidized OA, and some could be even included in the more oxidized OA.

A total of 15 experiments (including 2 blanks) were conducted during the SPRUCE-22 campaign, between July 7 and 25, 2022 (Table 2).

2.2 The dual chamber system

The experiments in both campaigns were conducted in the same dual-chamber system (Kaltsonoudis et al., 2019). The FORTH mobile chamber system (Fig. 1) consists of two identical PTFE chambers (1.3 m^3 each), five UV light panels (a total of 60 fluorescent 36 W lamps with a broad maximum at 365 nm, yielding a J_{NO2} of 0.1 min^{-1}) and several instruments for the measurement of the concentration of gases and particles inside the chambers. The instruments were sampling through a special port at the front side of each chamber. The two chambers and the light panels were located inside a hemispherical enclosure in order to protect them from rain, wind, etc. The top of the structure could be opened, if necessary, to expose them to natural sunlight or as a method of temperature control for the chambers. More details about the chamber setup and testing can be found in Kaltsonoudis et al. (2019). A metal-bellows pump (Senior Aerospace, model MB-302) was used to condition and fill the chambers with ambient air. Continuous measurements (1 min resolution) of temperature and relative humidity inside the chambers were performed in each experiment using two stainless-steel sensors (RH-USB, Omega).

2.3 Experimental procedure

The experimental procedure always started with the preparation of the chambers. Before each experiment the chambers were flushed continuously with ambient air for about 2 h using the metal-bellows pump, in order to condition them and the sampling lines with ambient air that will be used later for the actual experiment. During this period, an ionizer fan (Dr Schneider PC, Model SL-001) was used on the surface of the chamber walls for 20 min, in an effort to minimize the wall charges and thus the wall losses (Jorga et al., 2020). After this preparation procedure, the chambers were filled with ambient air while the synchronization of the different sampling instruments was performed. The concentration and chemical composition of the various gases and particles in both chambers was then characterized for 40 – 60 min. We measured the pollutant concentrations

in both chambers using an automated servo valve that was also synchronized with the sampling instruments. D9-butanol
160   (approximately 50-100 ppb) was injected in both chambers as an OH radical tracer to estimate from its decay the concentration
of the OH radicals. Then, nitrous acid (HONO) was bubbled in the perturbation chamber to produce OH radicals, while the
second one was used as a reference. The production of HONO was performed following the work of Mellouki and Mu (2003).
The line connecting the outlet of the bubbler to the perturbed chamber had a Teflon filter to prevent generated particles from
getting into the chamber. The dissociation of HONO together with the OH radicals, introduces high levels of NO (0.5-1 ppm)
165   in the perturbed chamber. The Po Valley is already in the high-NO_x regime, so this should have a small effect on the chemical
mechanisms of SOA formation. On the other hand, the same method in Pertouli introduces some uncertainty because the area
is generally characterized by low NO_x levels. Hydrogen peroxide (H_2O_2) was also used instead of HONO during four
experiments in Pertouli. The H_2O_2 was produced from a solution of hydrogen peroxide in water (50%-50%). The UV lights
were turned on after the HONO (or the H_2O_2) addition and the concentration of both gases and particles was followed for at
170   least 2-3 more hours. At the end of each experiment, ammonium sulfate seeds were injected using an atomizer to measure the
size dependent particle wall-loss rate constants following the work of Wang et al. (2018b). After the seed injection (an aqueous
solution of 5 g L^{-1} ammonium sulfate was used), the reduction of their concentration was measured for about 2 h. Finally, the
chambers were flushed again with ambient air to be ready for the next experiment.

2.4 Instrumentation

175   In both campaigns particle number size distributions in the range 14 – 700 nm were measured using a scanning mobility
particle sizer (SMPS, classifier model 3080, CPC models 3787 (FAIRARI) and 3775 (SPRUCE-22), DMA model 3081, TSI).
A High-Resolution Time-of-Flight Aerosol Mass Spectrometer (HR-ToF-AMS, Aerodyne) was used to monitor the sub-
micrometer particle chemical composition, mass size distribution and the organic aerosol mass spectrum. A suite of gas
monitors was used in both campaigns, including an O_3 monitor (model 400E, Teledyne), and a NO_x and NH_3 analyzer (model
180   T201, Teledyne). A Vocus CI-ToF mass spectrometer (Aerodyne Research Inc. and Tofwerk AG) was available during the Po
Valley experiments to measure the VOCs, but due to technical issues the quantification of the measured ion signals was not
possible. Also, a Proton-Transfer-Reaction Mass Spectrometer (PTR-MS 500, Ionicon) was used during the SPRUCE-22
campaign to measure the concentrations of volatile organic compounds.

During the FAIRARI campaign, all measuring instruments were located inside either the FAIRARI containers or the
185   FORTH mobile laboratory, which were both next to the chambers and had controlled temperature. During the SPRUCE-22
campaign the instruments were all inside the FORTH mobile laboratory. Quarter inch diameter copper (for particles) and PTFE
(for gases) sampling lines were used.

Simultaneous on-site ambient measurements were utilized during the Po Valley experiments, obtained from the CNR-
ISAC network and the Regional Agency for Prevention, Environment and Energy of Emilia-Romagna (ARPAE). The
190   instruments included an SO_2 (Model 43iTLE, Thermo Scientific), NO_x (Model 200A, Teledyne) and an NH_3 (Model 201E,

Teledyne) monitor. A meteorological station (Model WXT536, Vaisala Ltd) provided the various meteorological parameters in SPC. In Pertouli, ambient temperature and RH measurements were available.

2.5 Data analysis

The SeQUential Igor data RetRiEvaL (SQUIRREL) v1.57I and Peak Integration by Key Analysis (PIKA) v1.16I toolkits were
195 used for the analysis of the HR-ToF-AMS data in Igor Pro (Wave Metrics). The improved method by Canagaratna et al. (2015) was used to calculate the various elemental ratios. The Analytic Procedure for Elemental Separation (APES) software (Aiken et al., 2007; 2008) was used for the calculation of the O:C of the produced SOA in each experiment. The AMS data were corrected for the collection efficiency (CE) following the work of Kostenidou et al. (2007). The method compares the mass distributions obtained from the AMS with the volume size distributions of the SMPS and calculates the CE and the
200 corresponding density of the aerosol. Since the Po Valley experiments were conducted in an environment dominated by ammonium nitrate, the parameterization by Middlebrook et al. (2012) was also used to estimate the CE, accounting on the ammonium nitrate fraction. The comparison of the two methods is further discussed in the results section.

Following the work of Wang et al. (2018b) the size dependent wall-loss constant was estimated for each experiment, utilizing the decay of the concentration in the different size channels of the SMPS in the wall loss experiments.

205 To determine the OH concentration, we used the tracer method of Barmet et al. (2012). The reaction rate coefficient of d9-butanol with the OH radicals is equal to 3.42×10^{-12} cm^3 $molecule^{-1}$ s^{-1} (Barmet et al., 2012). The concentration of d9-butanol was measured by the PTR-MS in Pertouli with negligible interference by other organic compounds found in the atmosphere by observing changes at *m/z* 66. To measure the d-9 butanol decay in the Po Valley, the Vocus instrument signal (ions/s) was used, since the calculation of the OH radicals' concentration relies on the butanol's decay slope (Barmet et al.,
210 2012).

The mass spectra of the organic aerosol that was initially in the two chambers were always compared to verify that there were no significant artifacts during the filling process. The mass spectra of the OA were identical ($\theta < 5°$) in the two chambers in all experiments of both campaigns. Also, a comparison of the initial PM_1 and the O:C with the ambient values right before the start of each experiment was made. The O:C of the OA was practically the same inside the chambers and the
215 ambient. However, the PM_1 inside the chambers was 30-50% less than the ambient concentrations. This is mainly due to losses inside the pump used for filling the chambers and has been observed also in other similar studies (Jorga et al., 2020; 2021).

3 Results

3.1 Mass concentration corrections

3.1.1 Collection efficiency (CE) correction

220 The AMS collection efficiency in both campaigns ranged from 0.3 to 0.9 in all experiments. During the characterization period of each experiment (before the introduction of the HONO) in the Po Valley the CE was on average 0.35±0.13 while during the SOA formation period it increased to 0.7±0.19. This significant increase can be explained by the high production of ammonium nitrate observed in every experiment. It has been found that as the fraction of ammonium nitrate in PM_1 (in the current study it exceeded 75% in most experiments) increases, the CE tends to approach unity (Middlebrook et al., 2012). The relatively low

225 concentrations during the characterization period in some experiments resulted in noisy AMS size distributions (Fig. S2a), thus the corresponding loss corrections were more uncertain. Following the ammonium nitrate fraction-dependent CE parameterization developed by Middlebrook et al. (2012) the CE was found to be on average 0.5±0.09 for the period before the introduction of the OH radicals and 0.87±0.08 for the SOA formation period in the Po Valley experiments. While these values are reasonable, it is preferable to estimate the CE for each experiment based on the corresponding AMS and SMPS size

230 distribution measurements.

3.1.2 Wall loss correction

About 10 experiments with ammonium sulphate seeds took place in the Po Valley and another 7 in Pertouli, usually before or after the actual experiments. The wall loss dependent rate constants were measured for both chambers. An example of their dependence with the particle diameter is shown in Fig. S3 for a typical experiment in Po Valley. For particles with diameters

235 larger than 200 nm the rate constant was practically stable, and since the mass size distributions of the OA and the ammonium nitrate were always in the 300-800 nm size range (Fig. S4), the average wall loss rate constant in that range was used for the AMS measurements. This constant was on average 0.18 h^{-1} for both chambers. The wall loss constant was also estimated from the decay of sulphate's concentration in the control chamber during the actual experiments. This (size independent) wall-loss rate constant using this method was similar and had an average value of 0.2 h^{-1}.

240 ### 3.2 FAIRARI campaign (Po Valley)

3.2.1 Conditions during the FAIRARI campaign (Po Valley)

The period when the experiments were conducted (2 - 17 March 2022) was characterized by a relatively clean atmosphere for this area, with an average PM_1 equal to 13.3±7.9 μg m^{-3}, ranging from 3 to 40 μg m^{-3}. The main components of the ambient PM_1 were the organics and nitrates with an average concentration of 4.7±2.2 μg m^{-3} and 4.0±3.9 μg m^{-3}, respectively.

245 Ammonium (1.8±1.3 μg m^{-3}), sulfate (1.1±0.5 μg m^{-3}) and black carbon (1.5±0.7 μg m^{-3}) were also important components of the PM_1. Highly oxidized aerosol was present in the ambient during the experiment period, with an average O:C equal to 0.86.

NO_x ranged from 5 to 35 ppb with an average of 10 ppb during the measurement period, with an average concentration of NO_2 equal to 8±4.9 ppb and of NO 1.9±4.2 ppb. The concentration of ammonia was also high, ranging between 5 and 20 ppb, while ozone was on average 30±15 ppb, exhibiting a clear diurnal cycle peaking at 52 ppb.

250   The experiments started at different hours of the day (morning, noon, afternoon, and night) (Table 1) to investigate the SOA potential at different states of the atmospheric composition. As a result, the effect of different initial meteorological conditions was also investigated. Relatively low temperatures, in the range of 2-17 °C and high relative humidity (in the range of 30-80%) were measured during the period that the experiments took place. The initial concentration of OA ranged from 0.3 to 6 μg m^{-3}.

255   The diurnal profiles of both the meteorological parameters and the various PM_1 compounds measured by the AMS can be found in Fig. S5. Elevated concentrations of all pollutants and high humidity (about 80%) are observed during the nighttime and early morning hours, while the opposite is observed at noon.

3.2.2 Results of a typical perturbation experiment with high SOA formation

The initial PM_1 inside the chambers during Exp. 1 (started at 22:20 LT on 10/03/2022) was 15 μg m^{-3}. The organic aerosol had
260   a concentration of 4 μg m^{-3}, while nitrate (7 μg m^{-3}) and ammonium (3 μg m^{-3}) were also important fractions of the PM_1 mass (Fig. 2). The rest consisted mainly of sulfate (0.5 μg m^{-3}) and other species like chloride. The initial concentration of NO_2 inside the chambers was 7 ppb and of NO 9 ppb. Ozone had a concentration of 26 ppb at the beginning of the experiment. The initial temperature in the chambers (and also the ambient) was 5 °C and throughout the experiment it did not increase more than 2.5 °C. The initial RH was 76% and by the end of the experiment it had decreased to 60%.

265   Following the introduction of the HONO in the perturbed chamber (average OH in this experiment was 3.7×10^6 molecule cm^{-3}) and its illumination with UV (t = 0 h) rapid formation of SOA (Fig. 2a) was observed in the perturbed chamber. In the control, the concentration remained practically the same (within 10% of its initial value). The concentration of OA almost quadrupled, reaching 14 μg m^{-3} by the end (after 3.5 h) of the experiment. The formation rate of the organic aerosol in this experiment was 5.6 μg m^{-3} h^{-1}, for the first 2 h before its stabilization. No significant change in the concentration of sulfate
270   (Fig. 2b) was observed. The SO_2 was 0.12 ppb, and the expected sulfate formation based on the available OH was less than 0.05 μg m^{-3}.

An enormous increase of both the ammonium (Fig. 2c) and nitrate (Fig. 2d) concentrations was observed, indicating the production of ammonium nitrate inside the perturbed chamber. The concentration of nitrate reached 175 μg m^{-3} and of ammonium 54 μg m^{-3} by the end of the experiment. Although the NO_x concentrations inside the perturbed chamber were high
275   due to the HONO injection (NO of the order of 0.3-1 ppm), the formation of ammonium nitrate highlights the high concentration of the ambient gas phase ammonia in San Pietro Capofiume.

Regarding the gas phase, the NO concentration in the perturbed chamber immediately increased (Fig. S6a) as expected after the introduction of the OH radicals, stabilizing at 800 ppb. The ozone concentration decreased immediately (Fig. S6b)

after the HONO addition and UV illumination, from 26 ppb to 8 ppb in the perturbed chamber, while in the control it increased
280   by a few ppb by the end of the experiment.

3.2.3 Organic aerosol mass spectra

The initial mass spectra of both the control and the perturbed chambers were compared to ensure that there were no major differences in the OA. The θ angle between the two was 1°, suggesting identical OA. Notable differences (Fig. 3a) were observed between the mass spectra of the organic aerosol in the perturbed chamber before and after the SOA formation.
285   Examining the absolute values in the mass spectra, a significant increase was observed in m/z 18, 28 (CO^+) and 44 (CO_2^+) while a notable increase was also observed at m/z 27 ($C_2H_3^+$), 29 (CHO), 41 (C_3H_5), 47 ($CH_3O_2^+$), 48 (C_4^+), 55 ($C_4H_7^+$ and $C_3H_3O^+$) and 63 ($C_5H_3^+$). For m/z 47 and 48 interference by NO_2 containing molecules is possible. No notable decreases in the absolute m/z values were observed. The θ angle between the two spectra was 16°, suggesting significant differences in the perturbed chamber. On the other hand, the θ angle between the two spectra in the control chamber (Fig. 3b) was 2.5°, suggesting
290   practically identical spectra.

The mass spectra of the produced SOA in each experiment were estimated using the method introduced by Jorga et al. (2020). The method uses the mass balance of OA before and after its oxidation, assuming that the preexisting OA remains unchanged (negligible heterogeneous reactions). The approach uses the known wall loss rate constant to calculate the mass spectra of the formed SOA. More details and an example of this calculation can be found in Jorga et al. (2020). The major m/z
295   values of the produced SOA mass spectrum during Exp. 1 were 18, 28 and 44 (Fig. 3c). The θ angle between the produced SOA and the initial OA in the perturbation chamber was 18.9° suggesting significant changes in the spectrum.

The O:C ratio was initially (after the stabilization period) 0.7 in both chambers (Fig. 4), indicating an already highly oxidized aerosol. In the control chamber, the ratio remained unchanged for the first 2 h. A small decrease was observed after the second hour and at the end of the experiment O:C was equal to 0.63. The overall stable behavior of the O:C suggests that
300   the chemical evolution of the aerosol in the control chamber was limited, which is also confirmed by the mass spectra (Fig. 3b). On the other hand, in the perturbed chamber the O:C started increasing immediately after the production of the OH radicals and continued to do so for 1.5 h, when it stabilized at 1.05. The fact that the O:C increased by 0.35 (50% increase) highlights the potential of the Po Valley atmosphere to produce even more oxidized OA. The O:C of the produced SOA was equal to 1.1. This highlights the potential of this polluted atmosphere dominated by anthropogenic sources to form rapidly highly oxidized
305   SOA.

3.2.4 Results of other experiments in Po Valley

Formation of secondary organic aerosol was observed in the perturbed chamber in all experiments but one, while ammonium nitrate was always produced. Overall, the produced SOA ranged from 0.15 to 10 μg m^{-3} while the formation rate was ranging between 0.12 and 5.6 μg m^{-3} h^{-1} (Table 1) with an average of 1.9±1.8 μg m^{-3} h^{-1}. The concentration of the OH radicals inside
310   the perturbed chamber (after HONO injection and illumination with UV) was estimated to be in the range of 1-10×10^6

molecules cm^{-3}. A clear difference in the SOA formation potential was observed between daytime and nighttime experiments (Fig 5a). Higher potential of SOA formation was observed during the more polluted periods of the day (Fig. S5), indicating that along with the elevated PM$_1$ levels, elevated levels of VOCs were also present during the nighttime and early morning hours, when the formation potential maximized.

315 **Daytime experiments:** Experiments that took place during the day (7:00-19:00 LT) had a range of produced SOA between 0.15 and 1 μg m^{-3} with an average of 0.5 μg m^{-3}. The formation of ammonium nitrate ranged from 2.3 to 26.5 μg m^{-3}. During all the daytime experiments a significant drop in the concentration of the formed ammonium nitrate was observed, which was higher than the corresponding decay due to the wall losses. Given that this behavior was only observed in the daytime experiments, one explanation could be that they evaporated due to the higher temperatures during these periods. In these cases,
320 the temperature was ranging from 10 to 18 °C but for a given experiment the temperature change due to the UV illumination was never higher than 3-4 °C.

The experiment with no SOA formation (Exp. 2) also took place during daytime (at 13:30 LT on 7/3/2022). During this day, the ambient PM levels were low (PM$_1$ = 8 μg m^{-3}) but even in this case, 2.3 μg m^{-3} of ammonium nitrate was formed (Fig. S7) inside the perturbed chamber. The fact that there was at least one case when no detectable SOA was formed, acted
325 as another test of our system.

The average mass spectra of the organic aerosol at the beginning and the end of each experiment were compared to quantify the chemical evolution of the aerosol in both chambers. In the control chamber the spectra remained practically constant (θ<5°) during all experiments, except in the very low concentration Exp. 3 where the θ angle was 16° (both in the control and the perturbed chamber). At very low concentrations, interactions with the chamber walls can become significant and can affect the chemical profile of the aerosol. Comparing the mass spectra of the OA in the perturbed chamber before and
330 after the HONO injection, a relatively small θ angle in the range of 2–9° was calculated, suggesting that no significant changes took place during the daytime experiments.

The θ angle of the produced SOA mass spectra in the various daytime experiments in the Po Valley ranged between 5.2° and 15.5° with an average of 9.2±3.9°. This indicates that the formed SOA in these cases was quite similar with significant
335 signals at m/z 28, 29, 41, 43, 44, and 55 (Fig. S8a). Comparing the mass spectra of the produced SOA with the initial OA of the corresponding experiment, the θ angle ranged between 4° and 20° with an average of 11±6.7°. Therefore, this later generation SOA had some differences from the pre-existing OA.

The initial O:C during the daytime experiments ranged from 0.8 to 1.1 with an average of 1. Out of the 5 daytime experiments (excluding the two conducted during sunset and sunrise), the O:C increased only in one case (Exp. 4), where it
340 was initially 0.83 and reached 0.98 in the perturbed chamber at the end of the experiment (while in the control it remained stable). In all other cases the O:C remained within 10% of the initial value in both chambers (Fig. 5b). A decrease in the O:C was observed during the low concentration Exp. 3, which is consistent with the significant differences observed in the mass spectra of the organic aerosol. The O:C of the produced SOA during the daytime experiments was on average 1.05±0.13, ranging from 0.83 to 1.2.

345   Formation of new particles was observed in the perturbed chamber only during Exp. 3. The nucleation event (Fig. S9) started immediately after the production of the OH radicals (together with a small SOA formation of the order of 0.1 μg m^{-3}) and continued until the end of the experiment. What differentiated Exp. 3 from the others was the low ambient PM levels during that day. PM$_1$ was equal to 3 μg m^{-3} (campaign minimum), resulting in a low condensation sink, which favors (when the gaseous precursors are present) the formation of new particles (Kulmala et al., 2004).

350   **Nighttime experiments:** Experiments that took place during the night (19:00-7:00 LT) had a range of produced SOA between 0.75 and 10 μg m^{-3} with an average of 5.8 μg m^{-3} (Fig. 5a). The concentration of the formed ammonium nitrate ranged from 50 to 225 μg m^{-3}. The comparison of the organic aerosol mass spectra revealed that again in the control chamber there were minor changes ($\theta<5°$). In the perturbed, the θ angle ranged from 4° to 16° with an average of 10°, indicating that there were more changes compared to the daytime experiments. In all nighttime experiments, a significant increase was observed in the

355   m/z values 28 and 44 and 47, 48, 63 and their spectra were quite similar to the Exp. 1 described earlier.

The θ angle of the produced SOA mass spectra among the eight nighttime experiments in the Po Valley ranged between 2.4° and 19° with an average of 10.1±4.9°. This indicates that the formed SOA was quite similar in the nighttime experiments as well. The comparison of the formed SOA spectra between daytime and nighttime experiments showed that they were also quite similar. The θ angle ranged from 1° to 21° and had an average of 11.6±5.1°. The main fragments of the

360   formed SOA during the nighttime experiments were m/z 28 and 44 (Fig. S8b). Comparing the mass spectra of the produced SOA with the initial OA of the corresponding experiment, the θ angle ranged between 5.3° and 20° with an average of 11.8±5.1°.

The O:C ratio increased in all nighttime experiments (Fig. 5b) by 15±9% on average, reaching values as high as 1.05. This suggests that the oxidation cannot proceed much further than this limit in SPC. It is important to note that the initial O:C

365   during the night was lower (but still high) than in the daytime, with an average of 0.84 (while during the day it was close to 1). Experiments 6 and 7 were conducted close to sunrise (7:00 LT) and sunset (19:00 LT). These experiments were chemically closer to the nighttime ones, with relatively significant production of SOA and increase in the O:C. The O:C of the produced SOA during the nighttime experiments was on average 1±0.11, ranging from 0.77 to 1.1.

The results obtained by the nighttime experiments can be representative of the "polluted, humid conditions" that

370   dominate Po Valley during the fall and winter periods, even during daytime hours. Also, the insights from the more polluted (nighttime and early morning periods) can be used to elucidate what the contribution of the secondary material in the total PM levels would be, following the sunrise of the next day (and the natural formation of the OH radicals).

3.2.5 Dependence of the formed SOA on meteorological parameters and PM$_1$ levels.

The dependence of the formed organic and inorganic mass during each experiment on the meteorological parameters was

375   explored to understand their role in the corresponding processes. However, because the experiments took place at different hours and given that the examined variables vary systematically during the day (for example temperature is lower at night), it is difficult to arrive at robust conclusions about the net impact of each variable.

Higher SOA formation was observed (R^2=0.31) for the experiments that had higher relative humidity (Fig. 6a). This is also the case even if we separate the daytime and nighttime experiments. Conflicting results have been found in the literature regarding the effect of RH in SOA formation. A positive correlation has been found by various studies (Healy et al., 2009; White et al., 2014; Luo et al., 2019) as well as a negative correlation (Hinks et al., 2018; Jia and Xu, 2018; Zhang et al., 2019; Lamkaddam et al., 2020).

Temperature did not appear to affect the potential of SOA formation (Fig. 6b), at least directly (R^2=0.09), implying that other parameters controlled it.

The ambient PM_1 was overall connected (R^2=0.33) with higher SOA formation (Fig. 6c). A more polluted atmosphere implies higher concentrations of SOA precursors and a higher mass for partitioning of the produced semi volatile compounds. Unfortunately, measurements of VOCs and IVOCs were not available due to instrumentation problems.

3.2.6 Dependence of the formed ammonium nitrate on ambient ammonia levels.

A reasonable correlation (R^2=0.39) between the produced ammonium nitrate and the ambient ammonia right before the start of each experiment was found (Fig. 6d). An increasing concentration of gas phase NH_3 in the ambient resulted in higher NH_4NO_3 formation, confirming that its enormous concentrations in the chamber were partially due to the high ammonia content in SPC. The ratio between the produced nitrate and ammonium was always around 3.3 which is close to the molar mass ratio of the corresponding compounds (3.43).

3.3 SPRUCE-22 campaign (Pertouli)

3.3.1 Conditions during the SPRUCE-22 campaign

During the SPRUCE-22 campaign the levels of ambient PM_1 were comparable to those observed during the FAIRARI campaign, with an average of 12.7±5.1 µg m^{-3}, ranging between 0.7 and 27 µg m^{-3} (Matrali et al., 2024). Organics and sulfate were the dominant PM_1 components, having average concentrations equal to 7.4±3.2 µg m^{-3} and 3.8±1.7 µg m^{-3}, respectively. Ammonium (1.2 ±1.4 µg m^{-3}) and nitrate (0.1 ± 0.05 µg m^{-3}) had lower concentrations while black carbon also represented a small fraction of the PM_1 (0.26 ± 0.12 µg m^{-3}). Highly oxidized aerosol was present during the campaign, with an average O:C equal to 0.84.

Isoprene had an average concentration of 0.7 ± 1.1 ppb while monoterpenes were 0.5 ± 0.8 ppb (Matrali et al., 2024). The diurnal profile of isoprene peaked at around 15:00 LT reaching on average 2 ppb while the corresponding concentration of monoterpenes was 1 ppb. The concentrations of fresh anthropogenic pollutants were low. NO_2 concentration did not exceed 3.5 ppb and had an average of 1.8 ± 0.62 ppb while the anthropogenic VOCs also had small concentrations throughout the entire campaign. For instance, toluene had an average concentration of 0.002 ± 0.05 ppb and benzene 0.004 ± 0.03 ppb. However, a peak of the order of 0.05-0.1 ppb was observed at noon, examining the diurnal profile of the anthropogenic VOCs (Matrali et al., 2024). Ozone had a relatively stable concentration with an average of 64.8 ± 8.3 ppb.

The diurnal profiles of the meteorological parameters and the concentrations of the various species in the gas or
410   particulate phase can be found in Matrali et al. (2024).

3.3.2 Results of a perturbation experiment with SOA formation

The initial PM_1 inside the chambers during Exp. 1 (took place at 17:00 LT on 10/07/2022) was 6.6 μg m^{-3}. The organic aerosol
had a concentration of 3.1 μg m^{-3}, while sulfate was also an important fraction of the PM_1 with a concentration of 2.2 μg m^{-3}.
The rest consisted mainly of nitrate (0.3 μg m^{-3}), ammonium (0.8 μg m^{-3}) and other species like chloride. The initial
415   concentration of NO_2 inside the chambers was 1.4 ppb and of NO 2.4 ppb. Ozone had a concentration of 39 ppb at the beginning
of the experiment. The initial temperature in the chambers (and the ambient) was 19 °C and throughout the experiment it did
not increase by more than 3 °C. The initial RH was 66% and by the end of the experiment it had decreased to 55%.

Exp. 1 was the only experiment during the SPRUCE-22 campaign where clear formation of SOA was evident. Rapid
formation of SOA was observed in the perturbed chamber (Fig. 7a), right after the introduction of the OH radicals, while the
420   concentration of the organics in the control chamber remained constant. The concentration of the formed SOA was 1 μg m^{-3}
which corresponds to a 27% increase in the OA concentration while the SOA formation rate was equal to 1.1 μg m^{-3} h^{-1}. A
significant production of nitrates (about 20 μg m^{-3}) and ammonium (about 6 μg m^{-3}) also took place in the perturbed chamber.
The sulfate concentration (Fig. 7b) fluctuated between 2 – 2.5 μg m^{-3} in the perturbed chamber both before and after the
initiation of the photochemical reactions in this experiment, and overall, it remained practically constant.

425   The concentration of NO reached 300 ppb (Fig. S10a) in the perturbed chamber, following the introduction of HONO.
The concentration of OH radicals in the perturbed chamber was estimated to be equal to 2.2×10^6 molecules cm^{-3}. A decrease
in the concentration of O_3 (Fig. S10b) from 39 to 12 ppb was observed in the perturbation chamber after the introduction of
the OH radicals.

The available measurements of the various volatile organic compounds during the SPRUCE-22 campaign revealed
430   that during Exp. 1 the ambient isoprene and monoterpene concentrations were the highest recorded in all SPRUCE-22
experiments. Isoprene had a concentration of 2.4 ppb while for monoterpenes it was 1.1 ppb. The different behavior of Exp. 1
therefore could be partially explained by the higher availability of the monoterpenes and isoprene. At the same time, benzene
and toluene had a concentration of 0.08 ppb and 0.09 ppb, respectively, which was higher than the campaign averages at
midday (about 0.05 ppb for both compounds). Also, the relatively lower temperature should enhance the partitioning of the
435   products of the monoterpene reactions with OH towards the particulate phase. Notable is also the fact that this experiment took
place the day after a 2-day long rainy period occurred in Pertouli (midday of July 8 to morning of July 10, Matrali et al. (2024)).

3.3.3 Organic aerosol spectra

Comparing the OA mass spectra before and after the SOA formation in the perturbed chamber, signal increase was observed
in m/z 28 (CO^+), 44 (CO_2^+) and 63 (CH_3SO^+ and $CH_3O_3^+$). The θ angle between the two spectra was 8.7° (Fig. 8a), indicating

440   similar spectra with some differences. The θ angle between the corresponding spectra in the control chamber (Fig. 8b) was 6.6°, which can be explained by the notable drop of m/z 29.

        The major m/z values of the produced SOA mass spectrum during Exp. 1 were 28 and 44 (Fig. S11) while a smaller contribution of m/z 18, 27, 43 and 63 was also observed. The θ angle between the produced SOA and the initial OA in the perturbation chamber was 22.4° suggesting significant changes in the spectrum in this experiment.

445   The O:C was initially 0.8 in both chambers, implying highly oxidized organic aerosol. A small increase of 0.04 in the O:C was observed in the perturbed chamber after the introduction of the OH radicals (Fig. 9) suggesting that the OA in this experiment had some potential to further oxidize. The O:C in the control chamber had a decreasing pattern, reaching 0.7 by the end of the experiment. The O:C of the produced SOA was about 0.9.

3.3.4 Results of other experiments

450   Exp. 1 was the only experiment where clear SOA formation was observed in the perturbed chamber. The rest of the 12 experiments can be divided into two categories. The first includes experiments where formation of SOA was evident, but it could be observed for a limited amount of time (e.g. 15-30 min) and the second, experiments where no formation of SOA (nor ammonium nitrate) was detected.

        An example of the first category (Exp. 2) is depicted in Fig. S12. Although the concentration of the organics increased

455   in the perturbated chamber immediately after the production of OH radicals (reaching 2.5 μg m^{-3}, while the OA initially was 1.9 μg m^{-3}), it started decreasing after 15-30 min, and eventually reached its original value. The same behavior was observed for nitrates and ammonium. Given that both the organic aerosol and nitrates are semi-volatile, evaporation due to increasing temperature or vapor losses to the walls is a possible explanation. The hypothesis that this increase of the concentrations was due to the change of the collection efficiency of the AMS was also tested. However, volume concentrations measured by the

460   SMPS at the same time show an increase in concentrations in the perturbed chamber that is consistent with the increase measured by the AMS (Fig. S13). The fact that two independent instruments detected the same mass increase and decrease strongly suggests that this was not artifact due to the AMS operation. The most probable explanation was that this bump in concentration was due to incomplete mixing of the chamber. The formation reactions took place near the inlet of the reactor, higher concentrations existed in that region (from which the instruments were sampling) and then as the chamber was getting

465   mixed the concentrations decreased. Therefore, SOA was formed in these two cases, but its average concentration after the chamber was well mixed, was quite low (less than 0.1 μg m^{-3}) and could not be distinguished from the preexisting organic aerosol inside the chamber. The concentration of isoprene and monoterpenes in these experiments (1.6 ppb and 0.6 ppb for Exp. 2 and 1.3 ppb and 0.5 ppb for Exp. 3, respectively) were elevated compared to the experiments with no SOA (Fig. S14), but still lower than Exp. 1.

470   The rest of the HONO experiments and all the H$_2$O$_2$ experiments did not show any detectable increases in organic or nitrate aerosol concentrations. An example of such an experiment (Exp. 4, conducted on 20/7/2022) is depicted in Fig. 10. During these experiments, the ambient concentrations of isoprene and monoterpenes were considerably lower (they had

average concentrations of 1.2 ppb and 0.3 ppb, respectively) than in the ones in which some formation of SOA was evident. This highlights the importance of the biogenic vapors in the formation of SOA in Pertouli.

475   Although the anthropogenic compounds had higher than average concentration in two (out of three) experiments with SOA formation, there were at least 2 experiments where SOA did not form, with even higher concentrations of benzene and toluene (for example their concentration was 0.15 ppb and 0.07 ppb, respectively, at the beginning of Exp. 7 conducted on 23/07/2022). This suggests that the anthropogenic VOCs probably had a small contribution in SOA formation in Pertouli.

The initial O:C inside the chambers was on average 0.77±0.08 and did not vary significantly from one experiment to
480   another. The ratio remained practically stable in all experiments, excluding Exp. 1 where it increased by 0.04. During the experiments, when SOA was formed, PMF analysis (Paatero and Tapper, 1994) in the ambient revealed that the less oxidized organic aerosol factor (LO-OOA) was dominating while the more oxidized factor (MO-OOA) had low levels at the time (Vasilakopoulou et al., 2023). This indicates that the corresponding air masses were less aged. On the other hand, during the rest of the experiments, where no SOA formation was detected, the more oxidized OA factor was the dominant, suggesting
485   that the chemistry had progressed, and additional SOA production or oxidation were slow.

Except for the higher isoprene and monoterpene concentrations mentioned earlier, the three experiments where formation of SOA was evident had the highest initial relative humidities recorded (Table 2), in the range of 60-63%. These experiments were also characterized by lower temperatures (19-20 °C) compared to the rest.

3.4 Comparison of the two campaigns

490   The only experiment with SOA formation in Pertouli (Exp. 1) was compared to the experiments conducted in the Po Valley. The θ angle of the produced SOA mass spectra between this experiment and the corresponding ones in the Po Valley, was on average 11.9° ± 4.4°, ranging from 5.6° to 20°, indicating that the produced SOA had similarities in the two sites. Jimenez et al. (2009) found that the terminal oxidation of various sources often leads to similar AMS spectra, that are close to the factor LV-OOA. A comparison between the mass spectra of the SOA in Exp. 1 (Pertouli) and the average SOA mass spectra of the
495   daytime and nighttime experiments in the Po Valley is shown on Fig. S15.

The mass spectra of the produced SOA in the Po Valley and Pertouli (Exp. 1) were also compared to the LV-OOA (or the OOA-I) factor found in the ambient in various European campaigns during similar periods (spring-summer). The High-Resolution AMS Spectral Database (Ulbrich et al., 2009) was utilized. The mass spectra of the produced SOA in Po Valley were similar to the LV-OOA factor found in Rome during the DIAPASON campaign during May and June 2014 (Struckmeier
500   et al., 2016) with an average θ angle of 11.1°±3.3° (ranging from 6.3° to 17.6°). The corresponding theta angles for the SV-OOA in this study were on average 46.3°±4.9° (ranging from 39.2° to 54.4°). The produced SOA in Exp. 1 in Pertouli was also close to the LV-OOA of this study with a θ angle of 8.2° (while with the SV-OOA was 49.9°).

Similarities of the produced SOA in the Po Valley were also observed with the LV-OOA from Barcelona, March 2009 (Mohr et al., 2012) with an average θ angle of 13.8°±4.4° (ranging from 8.2° to 21°). The corresponding value for Exp.
505   1 in Pertouli was 18.6°. The comparison with the SV-OOA factor of this study showed again that it was quite different with

respect to the produced SOA mass spectra (the θ angles in this case were always higher than 30°). Finally, similar results were obtained comparing the experiments with the factor OOAa during April 2008 found in the Po Valley (Saarikoski et al., 2012) with an average θ angle of 14°±2.6° for the Po Valley experiments and 15.1° for Exp. 1 in Pertouli.

510 Positive Matrix Factorization (PMF) analysis was conducted using as input the AMS measurements obtained from the perturbed chamber of each experiment, to gain insights into the composition and evolution of the OA. Two factors were identified, one that was best described as LO-OOA, dominating in the beginning of each experiment, and the MO-OOA, dominating after the HONO injection. An example of the identified PMF factors is depicted in Fig. S16 for Exp. 1 in the Po Valley. The PMF analysis also confirmed the production of highly oxidized OA in our experiments.

515 Laboratory studies constitute the primary source of knowledge regarding the formation of SOA from anthropogenic VOCs (Srivastava et al., 2022). One of the limitations of these studies is that laboratory-produced SOA is far less oxidized than its counterpart in the ambient (Kroll and Seinfeld, 2008). The fact that in both campaigns, the produced OA was chemically closer to the more oxidized factors (LV-OOA, MO-OOA and OOAa, depending on the reference study) observed in the ambient than in laboratory studies, highlights the usefulness of such studies in understanding later generation chemical processes. The higher potential of SOA formation observed in the Po Valley (compared to Pertouli, where SOA was practically 520 formed in only one experiment) suggests that the anthropogenic VOCs have a higher potential to form later generation products, enhancing the mass of secondary material in the OA. Part of the explanation for the high SOA formation potential observed in the Po Valley could also be the contribution of less aged biomass burning OA emissions in this area (Saarikoski et al., 2012; Paglione et al., 2020), estimated to contribute about 25% of the OA during the FAIRARI campaign, compared to the very aged OA in Pertouli (Vasilakopoulou et al. 2023).

525 **4 Conclusions**

In this work we investigated the potential of ambient air in two different environments to form secondary organic aerosol (SOA) using a dual chamber system.

In the Po Valley a significant mass of SOA was formed rapidly (within the first hour) following the introduction of the OH radicals in the perturbed chamber. The produced SOA ranged between 0.1 and 10 µg m^{-3}. It was more than four times 530 higher than the initial OA in some nighttime experiments. Although the initial OA was already highly oxidized (O:C around 0.7-0.8) in all cases, its O:C increased to a maximum of 1.05, suggesting that later-generation-products with high O:C contribute much to the SOA in this environment. A positive correlation between the formed SOA and ambient RH and PM$_1$ levels was observed, suggesting that there is higher potential to form SOA under humid and polluted conditions, while there was not a clear connection with temperature. The high production of ammonium nitrate was connected to the elevated 535 concentrations of ambient ammonia.

On the other hand, infrequent and limited formation of SOA was observed during the SPRUCE-22 campaign. In the only experiment with clear SOA production, 1 µg m^{-3} of organic aerosol (27% increase) and 25 µg m^{-3} of ammonium nitrate

were formed in the perturbed chamber. This experiment was characterized by the highest ambient concentrations of isoprene and monoterpenes (2.4 ppb and 1.1 ppb, respectively) compared to the other experiments. The anthropogenic VOCs were

540 higher than the campaign average in this experiment but still much lower than the biogenic VOCs (toluene was 0.09 ppb and benzene 0.08 ppb). In two more experiments the formation of SOA was evident, but it disappeared 30 min after its formation, probably due to insufficient mixing of the chambers. The real SOA formed in these cases was probably below detection limit after the mixing. Our results in the SPRUCE-22 campaign suggest that under the conditions of the study (summertime in southeast Europe) the chemistry of the biogenic VOC-SOA system is quite fast and approaches its final state in the order of a

545 few hours or less. The ambient OA is quite oxidized (initial O:C around 0.75), the VOC concentrations are quite low due to their small lifetime, and the later generations of reactions contribute little to both the SOA mass concentration and its oxidation state. Since there was not any significant SOA production, the hypothesis that the behavior of the biogenic VOC-SOA system in this environment is consistent with the first or second-generation reactions and that any later generation production of SOA is of secondary importance appears to be valid.

550   A θ angle in the range of $5° – 21°$ was calculated comparing the mass spectra of the formed SOA in each experiment with the more oxidized OA factors (LV-OOA or OOAa) identified by various European field campaigns. This suggests that the formed SOA in both campaigns was similar to the more oxidized OA factors found in the ambient, which signifies the usefulness of such experiments in bridging laboratory experiments and real-world atmospheric conditions.

Altogether, although starting from a similar oxidation state (O:C=0.7-0.8), the atmosphere of the two sites has very

555 different potentials of forming SOA. In the Po Valley, the chemistry rapidly proceeds to form large amounts of SOA while in Pertouli the chemistry appears to have been terminated even before the beginning of most experiments, so the SOA formation practically does not proceed any further.

Competing interests. The contact author has declared that none of the authors has any competing interests.

560

Acknowledgements. This work has received funding from the European Union's Horizon 2020 research and innovation program through the projects FORCeS (grant agreement no. 821205) and ATMO-ACCESS (grant agreement no. 101008004) as well as by the Chemical evolution of gas and particulate-phase organic pollutants in the atmosphere (CHEVOPIN) project of the Hellenic Foundation for Research and Innovation (HFRI, grant agreement no. 1819). The authors also acknowledge the

565 help of Ghislain Motos and Athanasios Nenes for the completion of this work, the Regional Agency for Prevention, Environment and Energy of Emilia-Romagna (ARPAE) for providing the ambient data and the Stockholm University for providing the Vocus.

Author Contributions. AA performed the experiments in the Po Valley, analyzed the data from both campaigns and wrote

570 the paper, **DJS** performed the experiments at Pertouli and contributed to the data analysis, **CNV** contributed to the measurements and analyzed the AMS data, **AM**, **CK** and **AS** contributed to the measurements, **MP**, **MR** and **SD** helped with

the planning of the Po Valley experiments, provided the AMS and analyzed the ambient data, and **SNP** conceived and directed the study, synthesized the data and edited the paper.

References

575 Aiken, A. C., DeCarlo, P. F., and Jimenez, J. L.: Elemental analysis of organic species with electron ionization high-resolution mass spectrometry, Anal. Chem., 79, 8350–8358, https://doi.org/10.1021/ac071150w, 2007.

Aiken, A. C., DeCarlo, P. F., Kroll, J. H., Worsnop, D. R., Huffman, J. A., Docherty, K. S., Ulbrich, I. M., Mohr, C., Kimmel, J. R., Sueper, D., Sun, Y., Zhang, Q., Trimborn, A., Northway, M., Ziemann, P. J., Canagaratna, M. R., Onasch, T. B., Alfarra, M. R., Prevot, A. S. H., Dommen, J., Duplissy, J., Metzger, A., Baltensperger, U., and Jimenez, J. L.: O/C and

580 OM/OC ratios of primary, secondary, and ambient organic aerosols with high-resolution time-of-flight aerosol mass spectrometry, Environ. Sci. Technol., 42, 4478–4485, https://doi.org/10.1021/es703009q, 2008.

Barmet, P., Dommen, J., DeCarlo, P. F., Tritscher, T., Praplan, A. P., Platt, S. M., Prévôt, A. S. H., Donahue, N. M., and Baltensperger, U.: OH clock determination by proton transfer reaction mass spectrometry at an environmental chamber, Atmos. Meas. Tech., 5, 647–656, https://doi.org/10.5194/amt-5-647-2012, 2012.

585 Barreira, L. M. F., Ylisirniö, A., Pullinen, I., Buchholz, A., Li, Z., Lipp, H., Junninen, H., Hõrrak, U., Noe, S. M., Krasnova, A., Krasnov, D., Kask, K., Talts, E., Niinemets, Ü., Ruiz-Jimenez, J., and Schobesberger, S.: The importance of sesquiterpene oxidation products for secondary organic aerosol formation in a springtime hemiboreal forest, Atmos. Chem. Phys., 21, 11781–11800, https://doi.org/10.5194/acp-21-11781-2021, 2021.

Canagaratna, M. R., Jimenez, J. L., Kroll, J. H., Chen, Q., Kessler, S. H., Massoli, P., Hildebrandt Ruiz, L., Fortner, E.,

590 Williams, L. R., Wilson, K. R., Surratt, J. D., Donahue, N. M., Jayne, J. T., and Worsnop, D. R.: Elemental ratio measurements of organic compounds using aerosol mass spectrometry: characterization, improved calibration, and implications, Atmos. Chem. Phys., 15, 253–272, https://doi.org/10.5194/acp-15-253-2015, 2015.

Chan, A. W. H., Kautzman, K. E., Chhabra, P. S., Surratt, J. D., Chan, M. N., Crounse, J. D., Kürten, A., Wennberg, P. O., Flagan, R. C., and Seinfeld, J. H.: Secondary organic aerosol formation from photooxidation of naphthalene and

595 alkylnaphthalenes: implications for oxidation of intermediate volatility organic compounds (IVOCs), Atmos. Chem. Phys., 9, 3049–3060, https://doi.org/10.5194/acp-9-3049-2009, 2009.

Chaturvedi, S., Kumar, A., Singh, V., Chakraborty, B., Kumar, R., and Min, L.: Recent advancement in organic aerosol understanding: a review of their sources, formation, and health impacts, Water Air Soil Pollut., 234, 750, https://doi.org/10.1007/s11270-023-06772-0, 2023.

600 Daellenbach, K. R., Uzu, G., Jiang, J., Cassagnes, L.-E., Leni, Z., Vlachou, A., Stefenelli, G., Canonaco, F., Weber, S., Segers, A., Kuenen, J. J. P., Schaap, M., Favez, O., Albinet, A., Aksoyoglu, S., Dommen, J., Baltensperger, U., Geiser, M., El Haddad, I., Jaffrezo, J.-L., and Prévôt, A. S. H.: Sources of particulate-matter air pollution and its oxidative potential in Europe, Nature, 587, 414–419, https://doi.org/10.1038/s41586-020-2902-8, 2020.

Decesari, S., Allan, J., Plass-Duelmer, C., Williams, B. J., Paglione, M., Facchini, M. C., O'Dowd, C., Harrison, R. M., Gietl,
605   J. K., Coe, H., Giulianelli, L., Gobbi, G. P., Lanconelli, C., Carbone, C., Worsnop, D., Lambe, A. T., Ahern, A. T., Moretti,
        F., Tagliavini, E., Elste, T., Gilge, S., Zhang, Y., and Dall'Osto, M.: Measurements of the aerosol chemical composition
        and mixing state in the Po Valley using multiple spectroscopic techniques, Atmos. Chem. Phys., 14, 12109–12132,
        https://doi.org/10.5194/acp-14-12109-2014, 2014.

Docherty, K. S., Yaga, R., Preston, W. T., Jaoui, M., Reidel, T. P., Offenberg, J. H., Kleindienst, T. E., and Lewandowski, M.:
610   Relative contributions of selected multigeneration products to chamber SOA formed from photooxidation of a range (C_{10}–
        C_{17}) of n-alkanes under high NO_x conditions, Atmos. Environ., 244, 117976, https://doi.org/10.1016/
        j.atmosenv.2020.117976, 2021.

Donahue, N. M., Epstein, S. A., Pandis, S. N., and Robinson, A. L.: A two-dimensional volatility basis set: 1. organic-aerosol
        mixing thermodynamics, Atmos. Chem. Phys., 11, 3303–3318, https://doi.org/10.5194/acp-11-3303-2011, 2011.

615   Donahue, N. M., Henry, K. M., Mentel, T. F., Kiendler-Scharr, A., Spindler, C., Bohn, B., Brauers, T., Dorn, H. P., Fuchs, H.,
        Tillmann, R., Wahner, A., Saathoff, H., Naumann, K.-H., Möhler, O., Leisner, T., Müller, L., Reinnig, M.-C., Hoffmann,
        T., Salo, K., Hallquist, M., Frosch, M., Bilde, M., Tritscher, T., Barmet, P., Praplan, A. P., DeCarlo, P. F., Dommen, J.,
        Prévôt, A. S. H., and Baltensperger, U.: Aging of biogenic secondary organic aerosol via gas-phase OH radical reactions,
        Proc. Natl. Acad. Sci. U.S.A., 109, 13503–13508, https://doi.org/10.1073/pnas.1115186109, 2012.

620   European Environment Agency: Air quality in Europe 2022 – European Environment Agency (WWW Document),
        https://www.eea.europa.eu/publications/air-quality-in-europe-2022, 2022.

Griffin, R. J., Cocker III, D. R., Seinfeld, J. H., and Dabdub, D.: Estimate of global atmospheric organic aerosol from oxidation
        of biogenic hydrocarbons, Geophys. Res. Lett., 26, 2721–2724, https://doi.org/10.1029/1999GL900476, 1999a.

Griffin, R. J., Cocker III, D. R., Flagan, R. C., and Seinfeld, J. H.: Organic aerosol formation from the oxidation of biogenic
625   hydrocarbons, J. Geophys. Res. Atmos., 104, 3555–3567, https://doi.org/10.1029/1998JD100049, 1999b.

Guenther, A. B., Jiang, X., Heald, C. L., Sakulyanontvittaya, T., Duhl, T., Emmons, L. K., and Wang, X.: The Model of
        Emissions of Gases and Aerosols from Nature version 2.1 (MEGAN2.1): an extended and updated framework for modeling
        biogenic emissions, Geosci. Model Dev., 5, 1471–1492, https://doi.org/10.5194/gmd-5-1471-2012, 2012.

Harrison, D., Hunter, M. C., Lewis, A. C., Seakins, P. W., Bonsang, B., Gros, V., Kanakidou, M., Touaty, M., Kavouras, I.,
630   Mihalopoulos, N., Stephanou, E., Alves, C., Nunes, T., and Pio, C.: Ambient isoprene and monoterpene concentrations in
        a Greek fir (Abies Borisii-regis) forest. Reconciliation with emissions measurements and effects on measured OH
        concentrations, Atmos. Environ., 35, 4699–4711, https://doi.org/10.1016/S1352-2310(01)00091-7, 2001.

He, Q., Tomaz, S., Li, C., Zhu, M., Meidan, D., Riva, M., Laskin, A., Brown, S. S., George, C., Wang, X., and Rudich, Y.:
        Optical properties of secondary organic aerosol produced by nitrate radical oxidation of biogenic volatile organic
635   compounds, Environ. Sci. Technol., 55, 2878–2889, https://doi.org/10.1021/acs.est.0c06838, 2021.

Healy, R. M., Temime, B., Kuprovskyte, K., and Wenger, J. C.: Effect of relative humidity on gas/particle partitioning and aerosol mass yield in the photooxidation of p-xylene, Environ. Sci. Technol., 43, 1884–1889, https://doi.org/10.1021/es802404z, 2009.

Hinks, M. L., Montoya-Aguilera, J., Ellison, L., Lin, P., Laskin, A., Laskin, J., Shiraiwa, M., Dabdub, D., and Nizkorodov, S. A.: Effect of relative humidity on the composition of secondary organic aerosol from the oxidation of toluene, Atmos. Chem. Phys., 18, 1643–1652, https://doi.org/10.5194/acp-18-1643-2018, 2018.

Huang, R.-J., Zhang, Y., Bozzetti, C., Ho, K.-F., Cao, J.-J., Han, Y., Daellenbach, K. R., Slowik, J. G., Platt, S. M., Canonaco, F., Zotter, P., Wolf, R., Pieber, S. M., Bruns, E. A., Crippa, M., Ciarelli, G., Piazzalunga, A., Schwikowski, M., Abbaszade, G., Schnelle-Kreis, J., Zimmermann, R., An, Z., Szidat, S., Baltensperger, U., Haddad, I. E., and Prévôt, A. S. H.: High secondary aerosol contribution to particulate pollution during haze events in China, Nature, 514, 218–222, https://doi.org/10.1038/nature13774, 2014.

Ito, T., Bekki, K., Fujitani, Y., and Hirano, S.: The toxicological analysis of secondary organic aerosol in human lung epithelial cells and macrophages, Environ. Sci. Pollut. Res. Int., 26, 22747–22755, https://doi.org/10.1007/s11356-019-05317-5, 2019.

Jia, L. and Xu, Y.: Different roles of water in secondary organic aerosol formation from toluene and isoprene, Atmos. Chem. Phys., 18, 8137–8154, https://doi.org/10.5194/acp-18-8137-2018, 2018.

Jimenez, J. L., Canagaratna, M. R., Donahue, N. M., Prevot, A. S. H., Zhang, Q., Kroll, J. H., DeCarlo, P. F., Allan, J. D., Coe, H., Ng, N. L., Aiken, A. C., Docherty, K. S., Ulbrich, I. M., Grieshop, A. P., Robinson, A. L., Duplissy, J., Smith, J. D., Wilson, K. R., Lanz, V. A., Hueglin, C., Sun, Y. L., Tian, J., Laaksonen, A., Raatikainen, T., Rautiainen, J., Vaattovaara, P., Ehn, M., Kulmala, M., Tomlinson, J. M., Collins, D. R., Cubison, M. J., E., Dunlea, J., Huffman, J. A., Onasch, T. B., Alfarra, M. R., Williams, P. I., Bower, K., Kondo, Y., Schneider, J., Drewnick, F., Borrmann, S., Weimer, S., Demerjian, K., Salcedo, D., Cottrell, L., Griffin, R., Takami, A., Miyoshi, T., Hatakeyama, S., Shimono, A., Sun, J. Y., Zhang, Y. M., Dzepina, K., Kimmel, J. R., Sueper, D., Jayne, J. T., Herndon, S. C., Trimborn, A. M., Williams, L. R., Wood, E. C., Middlebrook, A. M., Kolb, C. E., Baltensperger, U., and Worsnop, D. R.: Evolution of organic aerosols in the atmosphere, Science, 326, 1525–1529, https://doi.org/10.1126/science.1180353, 2009.

Jo, Y., Jang, M., Han, S., Madhu, A., Koo, B., Jia, Y., Yu, Z., Kim, S., and Park, J.: CAMx–UNIPAR simulation of secondary organic aerosol mass formed from multiphase reactions of hydrocarbons under the Central Valley urban atmospheres of California, Atmos. Chem. Phys., 24, 487–508, https://doi.org/10.5194/acp-24-487-2024, 2024.

Jorga, S. D., Kaltsonoudis, C., Liangou, A., and Pandis, S. N.: Measurement of formation rates of secondary Aerosol in the ambient urban atmosphere using a dual smog chamber system, Environ. Sci. Technol., 54, 1336–1343, https://doi.org/10.1021/acs.est.9b03479, 2020.

Jorga, S. D., Florou, K., Kaltsonoudis, C., Kodros, J. K., Vasilakopoulou, C., Cirtog, M., Fouqueau, A., Picquet-Varrault, B., Nenes, A., and Pandis, S. N.: Nighttime chemistry of biomass burning emissions in urban areas: A dual mobile chamber study, Atmos. Chem. Phys., 21, 15337–15349, https://doi.org/10.5194/acp-21-15337-2021, 2021.

670   Kaltsonoudis, C., Jorga, S. D., Louvaris, E., Florou, K., and Pandis, S. N.: A portable dual-smog-chamber system for atmospheric aerosol field studies, Atmos. Meas. Tech., 12, 2733–2743, https://doi.org/10.5194/amt-12-2733-2019, 2019.

Kanakidou, M., Seinfeld, J. H., Pandis, S. N., Barnes, I., Dentener, F. J., Facchini, M. C., Van Dingenen, R., Ervens, B., Nenes, A., Nielsen, C. J., Swietlicki, E., Putaud, J. P., Balkanski, Y., Fuzzi, S., Horth, J., Moortgat, G. K., Winterhalter, R., Myhre, C. E. L., Tsigaridis, K., Vignati, E., Stephanou, E. G., and Wilson, J.: Organic aerosol and global climate modelling: a
675   review, Atmos. Chem. Phys., 5, 1053–1123, https://doi.org/10.5194/acp-5-1053-2005, 2005.

Kerminen, V.-M., Chen, X., Vakkari, V., Petäjä, T., Kulmala, M., and Bianchi, F.: Atmospheric new particle formation and growth: review of field observations, Environ. Res. Lett., 13, 103003, https://doi.org/10.1088/1748-9326/aadf3c, 2018.

Kostenidou, E., Pathak, R. K., and Pandis, S. N.: An algorithm for the calculation of secondary organic aerosol density combining AMS and SMPS data, Aerosol Sci. Tech., 41, 1002–1010, https://doi.org/10.1080/02786820701666270, 2007.

680   Kroll, J. H. and Seinfeld, J. H.: Chemistry of secondary organic aerosol: Formation and evolution of low-volatility organics in the atmosphere, Atmos. Environ., 42, 3593–3624, https://doi.org/10.1016/j.atmosenv.2008.01.003, 2008.

Kroll, J. H., Ng, N. L., Murphy, S. M., Flagan, R. C., and Seinfeld, J. H.: Secondary organic aerosol formation from isoprene photooxidation, Environ. Sci. Technol., 40, 1869–1877, https://doi.org/10.1021/es0524301, 2006.

Kulmala, M., Vehkamäki, H., Petäjä, T., Maso, M. D., Lauri, A., Kerminen, V. M., Birmili, W., and McMurry, P. H.:
685   Formation and growth rates of ultrafine atmospheric particles: A review of observations, J. Aerosol Sci., 35, 143–176, https://doi.org/10.1016/j.jaerosci.2003.10.003, 2004.

Lamkaddam, H., Gratien, A., Pangui, E., David, M., Peinado, F., Polienor, J.-M., Jerome, M., Cazaunau, M., Gaimoz, C., Picquet-Varrault, B., Kourtchev, I., Kalberer, M., and Doussin, J.-F.: Role of relative humidity in the secondary organic aerosol formation from high-NO_x photooxidation of long-chain alkanes: n-dodecane case study, ACS Earth Space Chem.,
690   4, 2414–2425, https://doi.org/10.1021/acsearthspacechem.0c00265, 2020.

Lim, Y. B. and Ziemann, P. J.: Effects of molecular structure on aerosol yields from OH radical-initiated Reactions of linear, branched, and cyclic alkanes in the presence of NO_x, Environ. Sci. Technol., 43, 2328–2334, https://doi.org/10.1021/es803389s, 2009.

Luo, H., Jia, L., Wan, Q., An, T., and Wang, Y.: Role of liquid water in the formation of O3 and SOA particles from 1,2,3-
695   trimethylbenzene, Atmos. Environ., 217, 116955, https://doi.org/10.1016/j.atmosenv.2019.116955, 2019.

Matrali, A., Vasilakopoulou, C. N., Aktypis A., Kaltsonoudis, C., Florou, K., Błaziak, A., Patoulias, D., Kostenidou, E., Błaziak, K., Seitanidi K., Skyllakou, K., Fagault Y., Tuna T., Panagiotopoulos C., Bard B., Nenes A. and Pandis, S. N.: Anthropogenic and biogenic pollutants in a forested environment: SPRUCE-22 campaign overview, 2024. (under review)

Mellouki, A. and Mu, Y.: On the atmospheric degradation of pyruvic acid in the gas phase, J. Photochem. Photobiol., A, 157,
700   295–300, https://doi.org/10.1016/S1010-6030(03)00070-4, 2003.

Middlebrook, A. M., Bahreini, R., Jimenez, J. L., and Canagaratna, M. R.: Evaluation of composition-dependent collection efficiencies for the aerodyne aerosol mass spectrometer using field data, Aerosol Sci. Tech., 46, 258–271, https://doi.org/10.1080/02786826.2011.620041, 2012.

Mohr, C., DeCarlo, P. F., Heringa, M. F., Chirico, R., Slowik, J. G., Richter, R., Reche, C., Alastuey, A., Querol, X., Seco, R.,
705   Peñuelas, J., Jiménez, J. L., Crippa, M., Zimmermann, R., Baltensperger, U., and Prévôt, A. S. H.: Identification and
    quantification of organic aerosol from cooking and other sources in Barcelona using aerosol mass spectrometer data,
    Atmos. Chem. Phys., 12, 1649–1665, https://doi.org/10.5194/acp-12-1649-2012, 2012.

Müller, L., Reinnig, M.-C., Naumann, K. H., Saathoff, H., Mentel, T. F., Donahue, N. M., and Hoffmann, T.: Formation of 3-
    methyl-1,2,3-butanetricarboxylic acid via gas phase oxidation of pinonic acid – a mass spectrometric study of SOA aging,
710   Atmos. Chem. Phys., 12, 1483–1496, https://doi.org/10.5194/acp-12-1483-2012, 2012.

Nault, B. A., Jo, D. S., McDonald, B. C., Campuzano-Jost, P., Day, D. A., Hu, W., Schroder, J. C., Allan, J., Blake, D. R.,
    Canagaratna, M. R., Coe, H., Coggon, M. M., DeCarlo, P. F., Diskin, G. S., Dunmore, R., Flocke, F., Fried, A., Gilman, J.
    B., Gkatzelis, G., Hamilton, J. F., Hanisco, T. F., Hayes, P. L., Henze, D. K., Hodzic, A., Hopkins, J., Hu, M., Huey, L.
    G., Jobson, B. T., Kuster, W. C., Lewis, A., Li, M., Liao, J., Nawaz, M. O., Pollack, I. B., Peischl, J., Rappenglück, B.,
715   Reeves, C. E., Richter, D., Roberts, J. M., Ryerson, T. B., Shao, M., Sommers, J. M., Walega, J., Warneke, C., Weibring,
    P., Wolfe, G. M., Young, D. E., Yuan, B., Zhang, Q., de Gouw, J. A., and Jimenez, J. L.: Secondary organic aerosols from
    anthropogenic volatile organic compounds contribute substantially to air pollution mortality, Atmos. Chem. Phys., 21,
    11201–11224, https://doi.org/10.5194/acp-21-11201-2021, 2021.

Ng, N. L., Kroll, J. H., Keywood, M. D., Bahreini, R., Varutbangkul, V., Flagan, R. C., Seinfeld, J. H., Lee, A., and Goldstein,
720   A. H.: Contribution of first- versus second-generation products to secondary organic aerosols formed in the oxidation of
    biogenic hydrocarbons, Environ. Sci. Technol., 40, 2283–2297, https://doi.org/10.1021/es052269u, 2006.

Neuberger, A., Decesari, S., Aktypis, A., Andersen, H., Baumgardner, D., Bianchi, F., Busetto, M., Cai, J., Cermak, J., Dipu,
    J., Ekman, A., Fuzzi, S., Gramlich, Y., Hadden, D., Haslett, S. L., Heikkinen, L., Joutsensaari, J., Kaltsonoudis, C.,
    Kangasluoma, J., Lupi, A., Marinoni, A., Matrali, A., Mattsson, F., Mohr, M., Nenes, A., Paglione, M., Pandis, S. N., Patel,
725   A., Riipinen, I., Rinaldi, M., Steimer, S. S., Stolzenburg, D., Sulo, J., Vasilakopoulou, C. N., Zieger, P.: From molecules
    to droplets: The Fog and Aerosol InteRAction Research Italy (FAIRARI) 2021/22 campaign, Bulletin of the American
    Meteorological Society, 2024. (under review)

Paatero, P. and Tapper, U.: Positive matrix factorization: A non-negative factor model with optimal utilization of error
    estimates of data values, Environmetrics, 5, 111–126, https://doi.org/10.1002/env.3170050203, 1994.

730 Paglione, M., Gilardoni, S., Rinaldi, M., Decesari, S., Zanca, N., Sandrini, S., Giulianelli, L., Bacco, D., Ferrari, S., Poluzzi,
    V., Scotto, F., Trentini, A., Poulain, L., Herrmann, H., Wiedensohler, A., Canonaco, F., Prévôt, A. S. H., Massoli, P.,
    Carbone, C., Facchini, M. C., and Fuzzi, S.: The impact of biomass burning and aqueous-phase processing on air quality:
    a multi-year source apportionment study in the Po Valley, Italy, Atmos. Chem. Phys., 20, 1233–1254,
    https://doi.org/10.5194/acp-20-1233-2020, 2020.

735 Paglione, M., Decesari, S., Rinaldi, M., Tarozzi, L., Manarini, F., Gilardoni, S., Facchini, M. C., Fuzzi, S., Bacco, D., Trentini,
    A., Pandis, S. N., and Nenes, A.: Historical changes in seasonal aerosol acidity in the Po Valley (Italy) as inferred from

fog water and aerosol measurements, Environ. Sci. Technol., 55, 7307–7315, https://doi.org/10.1021/acs.est.1c00651, 2021.

Pavlidis, D., Sippial, D. J., Florou, K., Kostenidou, E., and Pandis, S. N.: Exploring the discrepancies between SMPS and AMS measurements in secondary organic aerosol formation experiments, Aerosol Sci. Tech., 58, 195–205, https://doi.org/10.1080/02786826.2024.2304547, 2024.

Pope III, C. A. and Dockery, D. W.: Health Effects of Fine Particulate Air Pollution: Lines that Connect, J. Air Waste Manag. Assoc., 56, 709–742, https://doi.org/10.1080/10473289.2006.10464485, 2006.

Presto, A. A., Miracolo, M. A., Donahue, N. M., and Robinson, A. L.: Secondary organic aerosol formation from high-NO_x photo-oxidation of low volatility precursors: n-alkanes, Environ. Sci. Technol., 44, 2029–2034, https://doi.org/10.1021/es903712r, 2010.

Qi, L., Nakao, S., and Cocker III, D. R.: Aging of secondary organic aerosol from α-pinene ozonolysis: Roles of hydroxyl and nitrate radicals, J. Air Waste Manag. Assoc., 62, 1359–1369, https://doi.org/10.1080/10962247.2012.712082, 2012.

Robinson, A. L., Donahue, N. M., Shrivastava, M. K., Weitkamp, E. A., Sage, A. M., Grieshop, A. P., Lane, T. E., Pierce, J. R., and Pandis, S. N.: Rethinking organic aerosols: semivolatile emissions and photochemical aging, Science, 315, 1259–1262, https://doi.org/10.1126/science.1133061, 2007.

Saarikoski, S., Carbone, S., Decesari, S., Giulianelli, L., Angelini, F., Canagaratna, M., Ng, N. L., Trimborn, A., Facchini, M. C., Fuzzi, S., Hillamo, R., and Worsnop, D.: Chemical characterization of springtime submicrometer aerosol in Po Valley, Italy, Atmos. Chem. Phys., 12, 8401–8421, https://doi.org/10.5194/acp-12-8401-2012, 2012.

Seinfeld, J. H. and Pandis, S. N.: Atmospheric Chemistry and Physics from Air Pollution to Climate Change, John Wiley, Hoboken, NJ, ISBN 978-1-118-94740-1, 2016.

Squizzato, S., Masiol, M., Brunelli, A., Pistollato, S., Tarabotti, E., Rampazzo, G., and Pavoni, B.: Factors determining the formation of secondary inorganic aerosol: a case study in the Po Valley (Italy), Atmos. Chem. Phys., 13, 1927–1939, https://doi.org/10.5194/acp-13-1927-2013, 2013.

Srivastava, D., Vu, T. V., Tong, S., Shi, Z., and Harrison, R. M.: Formation of secondary organic aerosols from anthropogenic precursors in laboratory studies, NPJ Clim. Atmos. Sci., 5, 1–30, https://doi.org/10.1038/s41612-022-00238-6, 2022.

Struckmeier, C., Drewnick, F., Fachinger, F., Gobbi, G. P., and Borrmann, S.: Atmospheric aerosols in Rome, Italy: sources, dynamics and spatial variations during two seasons, Atmos. Chem. Phys., 16, 15277–15299, https://doi.org/10.5194/acp-16-15277-2016, 2016.

Tasoglou, A. and Pandis, S. N.: Formation and chemical aging of secondary organic aerosol during the β-caryophyllene oxidation, Atmos. Chem. Phys., 15, 6035–6046, https://doi.org/10.5194/acp-15-6035-2015, 2015.

Tkacik, D. S., Presto, A. A., Donahue, N. M., and Robinson, A. L.: Secondary organic aerosol formation from intermediate-volatility organic compounds: Cyclic, linear, and branched alkanes, Environ. Sci. Technol., 46, 8773–8781, https://doi.org/10.1021/es301112c, 2012.

770 Tsigaridis, K., Daskalakis, N., Kanakidou, M., Adams, P. J., Artaxo, P., Bahadur, R., Balkanski, Y., Bauer, S. E., Bellouin, N., Benedetti, A., Bergman, T., Berntsen, T. K., Beukes, J. P., Bian, H., Carslaw, K. S., Chin, M., Curci, G., Diehl, T., Easter, R. C., Ghan, S. J., Gong, S. L., Hodzic, A., Hoyle, C. R., Iversen, T., Jathar, S., Jimenez, J. L., Kaiser, J. W., Kirkevåg, A., Koch, D., Kokkola, H., Lee, Y. H., Lin, G., Liu, X., Luo, G., Ma, X., Mann, G. W., Mihalopoulos, N., Morcrette, J.-J., Müller, J.-F., Myhre, G., Myriokefalitakis, S., Ng, N. L., O'Donnell, D., Penner, J. E., Pozzoli, L., Pringle,

775 K. J., Russell, L. M., Schulz, M., Sciare, J., Seland, Ø., Shindell, D. T., Sillman, S., Skeie, R. B., Spracklen, D., Stavrakou, T., Steenrod, S. D., Takemura, T., Tiitta, P., Tilmes, S., Tost, H., van Noije, T., van Zyl, P. G., von Salzen, K., Yu, F., Wang, Z., Zaveri, R. A., Zhang, H., Zhang, K., Zhang, Q., and Zhang, X.: The AeroCom evaluation and intercomparison of organic aerosol in global models, Atmos. Chem. Phys., 14, 10845–10895, https://doi.org/10.5194/acp-14-10845-2014, 2014.

780 Ulbrich, I. M., Canagaratna, M. R., Zhang, Q., Worsnop, D. R., and Jimenez, J. L.: Interpretation of organic components from Positive Matrix Factorization of aerosol mass spectrometric data, Atmos. Chem. Phys., 9, 2891–2918, https://doi.org/10.5194/acp-9-2891-2009, 2009.

Vasilakopoulou, C. N., Matrali, A., Skyllakou, K., Georgopoulou, M., Aktypis, A., Florou, K., Kaltsonoudis, C., Siouti, E., Kostenidou, E., Błaziak, A., Nenes, A., Papagiannis, S., Eleftheriadis, K., Patoulias, D., Kioutsioukis, I., and Pandis, S. N.:
785 Rapid transformation of wildfire emissions to harmful background aerosol, NPJ Clim. Atmos. Sci., 6, 1–9, https://doi.org/10.1038/s41612-023-00544-7, 2023.

Volkamer, R., Jimenez, J. L., San Martini, F., Dzepina, K., Zhang, Q., Salcedo, D., Molina, L. T., Worsnop, D. R., and Molina, M. J.: Secondary organic aerosol formation from anthropogenic air pollution: Rapid and higher than expected, Geophys. Res. Lett., 33, https://doi.org/10.1029/2006GL026899, 2006.

790 Wang, N., Kostenidou, E., Donahue, N. M., and Pandis, S. N.: Multi-generation chemical aging of α-pinene ozonolysis products by reactions with OH, Atmos. Chem. Phys., 18, 3589–3601, https://doi.org/10.5194/acp-18-3589-2018, 2018a.

Wang, N., Jorga, S. D., Pierce, J. R., Donahue, N. M., and Pandis, S. N.: Particle wall-loss correction methods in smog chamber experiments, Atmos. Meas. Tech., 11, 6577–6588, https://doi.org/10.5194/amt-11-6577-2018, 2018b.

White, S. J., Jamie, I. M., and Angove, D. E.: Chemical characterisation of semi-volatile and aerosol compounds from the
795 photooxidation of toluene and NO$_x$, Atmos. Environ., 83, 237–244, https://doi.org/10.1016/j.atmosenv.2013.11.023, 2014.

Zhang, Q., Xu, Y., and Jia, L.: Secondary organic aerosol formation from OH-initiated oxidation of m-xylene: effects of relative humidity on yield and chemical composition, Atmos. Chem. Phys., 19, 15007–15021, https://doi.org/10.5194/acp-19-15007-2019, 2019.

Zhao, Y., Hennigan, C. J., May, A. A., Tkacik, D. S., de Gouw, J. A., Gilman, J. B., Kuster, W. C., Borbon, A., and Robinson,
800 A. L.: Intermediate-volatility organic compounds: A large source of secondary organic aerosol, Environ. Sci. Technol., 48, 13743–13750, https://doi.org/10.1021/es5035188, 2014.

Table 1: Starting times, initial conditions and total SOA formed and SOA formation rate of each experiment conducted during the FAIRARI campaign.

Experiment	Starting time (LT)	RH (%)	Temperature (°C)	Initial OA (µg m⁻³)	Initial O:C	SOA formed (µg m⁻³)	SOA formation rate (µg m⁻³ h⁻¹)
1	22:20	76	5	3.8	0.77	10.0	5.6
2	13:30	33	17	1.7	1.09	0	0
3	14:10	36	11	0.3	0.98	0.2	0.1
4	9:00	50	6	0.7	0.84	0.6	1.2
5	16:20	33	13	1.4	1.1	0.2	0.1
6	7:10	65	2	2.3	0.73	0.8	0.8
7	19:00	35	8	1.8	0.78	4.5	4.5
8	16:30	30	16	0.9	0.95	0.6	0.6
9	12:20	40	14	2.2	0.99	0.4	0.4
10	0:20	73	5	2.1	1.03	4.2	3.9
11	20:20	65	8	2.1	0.93	2.6	2.0
12	19:00	67	8	2.4	0.85	0.8	1.5
13	5:00	78	4	1.7	0.77	2.0	1.5
14	20:10	60	10	6.5	0.86	2.7	3.7
Blank	20:10	60	10	6.5	0.86	-	-
Blank	13:30	42	11	4.0	1.1	-	-

805

Table 2: Starting times and initial conditions of each experiment conducted during the SPRUCE-22 campaign.

Experiment	Starting time (LT)	RH (%)	Temperature (°C)	Initial OA (µg m⁻³)	Initial O:C	Oxidant
1	16:55	62	19	2.9	0.76	HONO
2	11:30	60	19.5	1.8	0.74	HONO
3	11:10	60	20	1.8	0.65	HONO
4	14:15	52	23	4.7	0.83	H_2O_2
5	9:55	54	21	3.7	0.76	HONO
6	15:25	33	31	2.7	0.83	HONO
7	14:40	36	30	3	0.82	HONO
8	11:50	31	29	3.7	0.81	HONO
9	11:40	48	25	4.2	0.81	HONO
10	11:20	63	20	2.4	0.85	H_2O_2
11	15:05	63	21	2.7	0.55	HONO
12	11:25	47	22	2.9	0.82	H_2O_2
13	11:50	45	25	3.4	0.83	H_2O_2
Blank	12:00	55	18	2.0	0.86	-
Blank	10:10	50	23	4.7	0.77	-
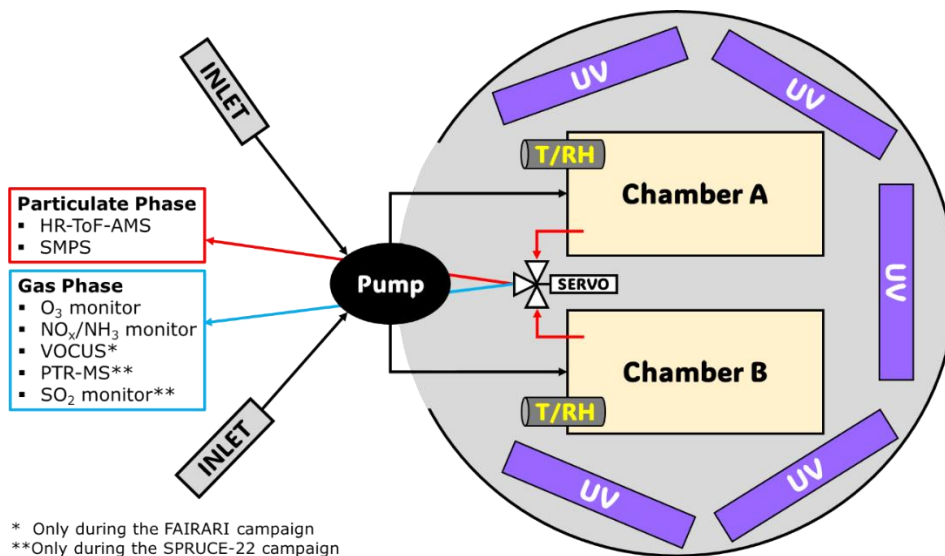
Figure 1: Schematic of the experimental setup used in both campaigns.

810
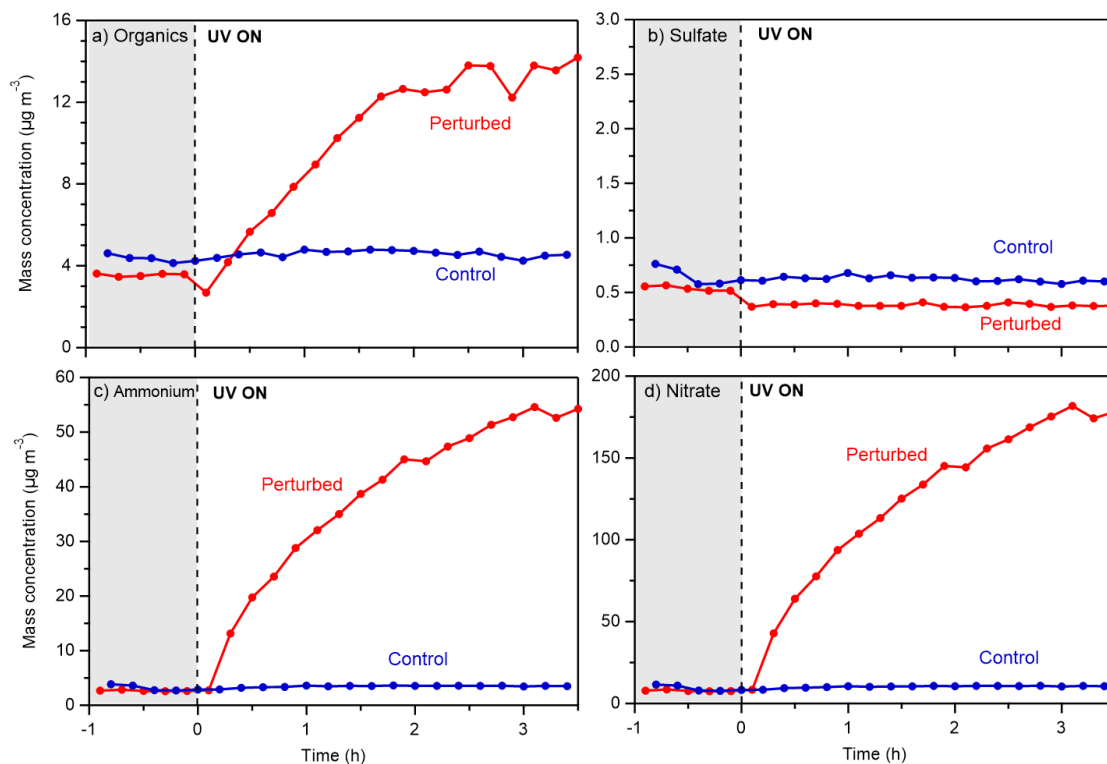
Figure 2: Wall-loss and CE corrected mass concentrations of a) organics, b) sulfate, c) ammonium and d) nitrate in the perturbed and the control chambers during the nighttime Exp. 1 in Po Valley.
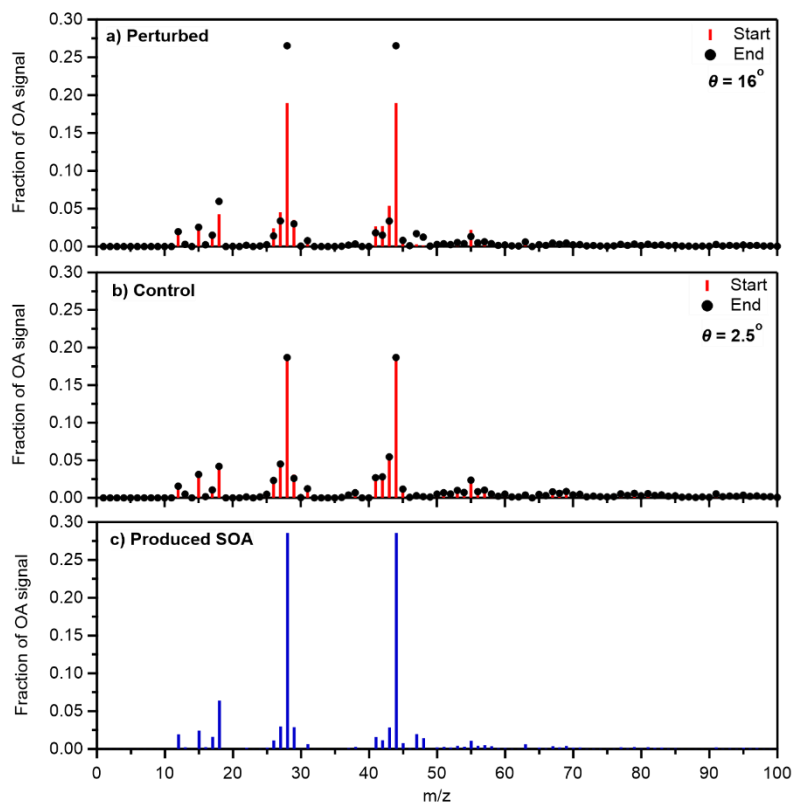
Figure 3: Average fractional signal of the organic aerosol at the start and the end of Exp. 1 in Po Valley in a) the perturbed and b) the control chambers. The mass spectrum of the SOA formed in the perturbed chamber during the same experiment (c) is also depicted.
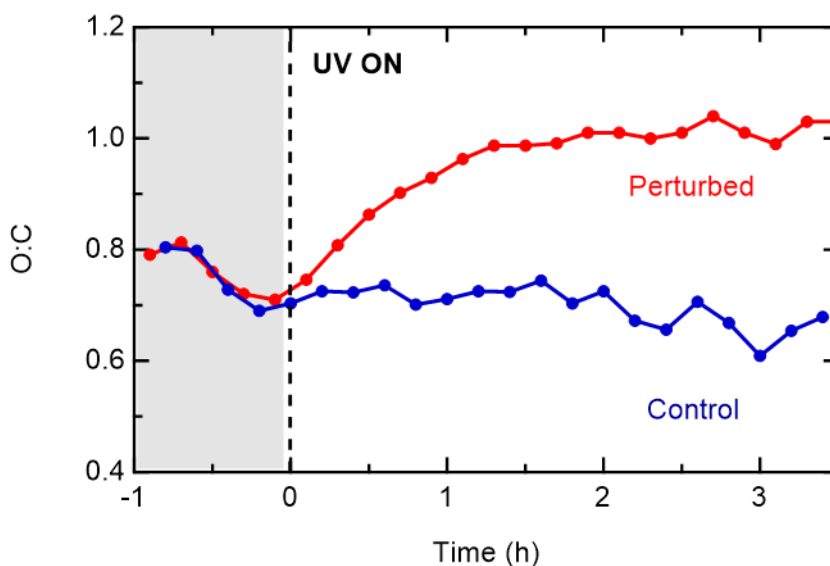
Figure 4: Evolution of the O:C inside the perturbed and the control chambers during Exp. 1 in Po Valley.

820
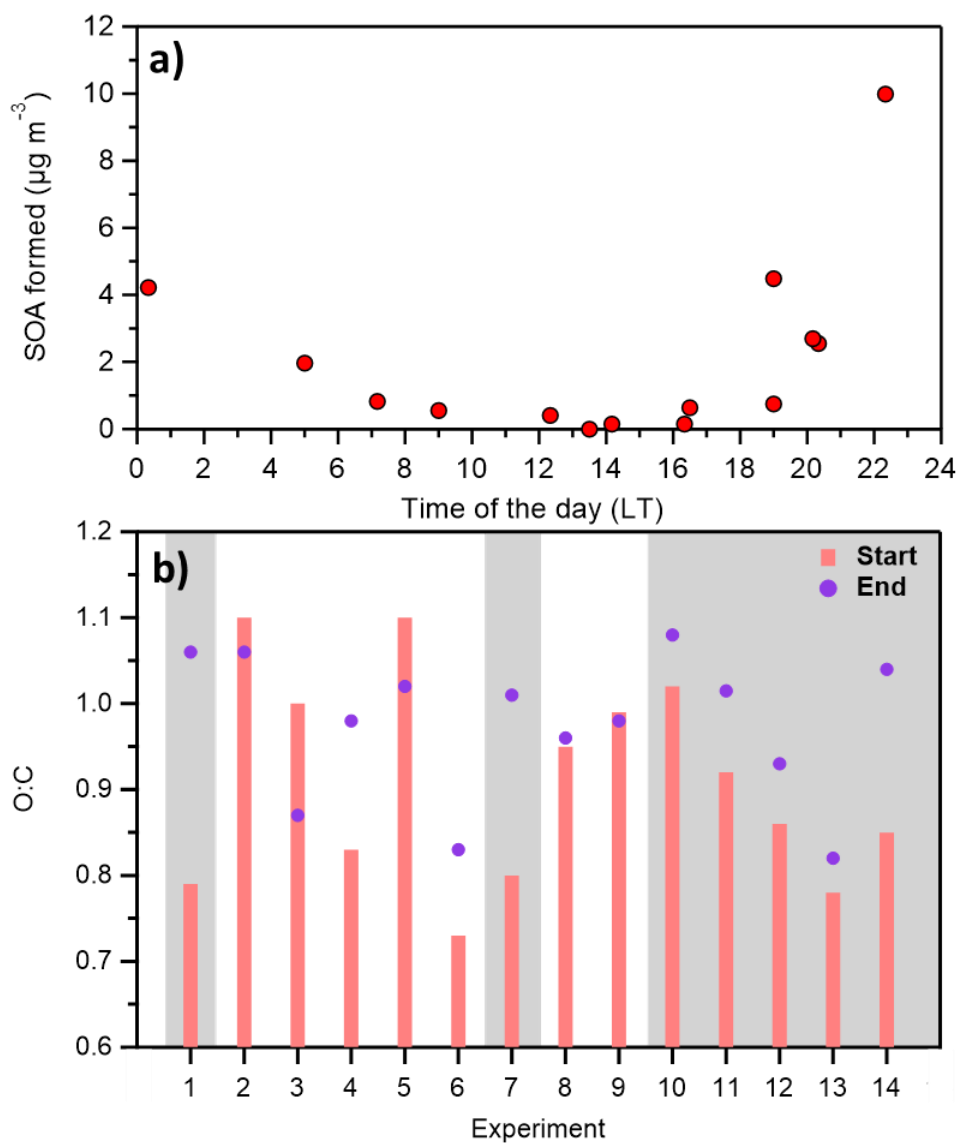
Figure 5: a) The SOA formed in each experiment in the Po Valley together with its corresponding starting time and b) The average O:C at the beginning and the end of each experiment. The grey areas denote the nighttime experiments.
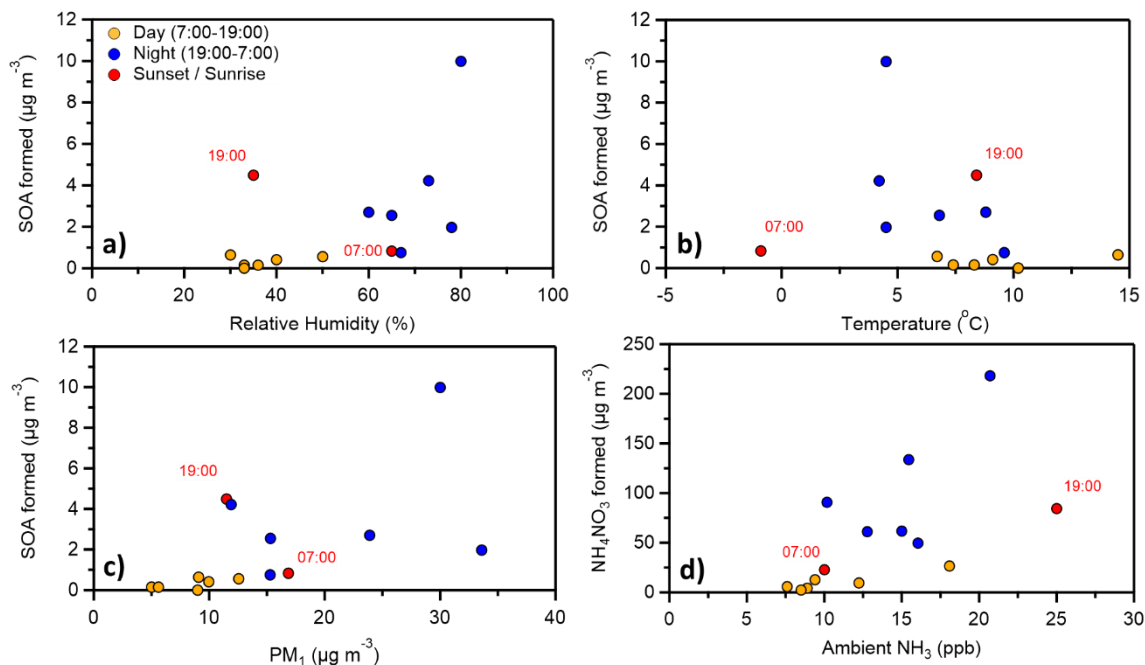
Figure 6: The mass concentration of the formed SOA (raw data) in each experiment together with the ambient a) relative humidity, b) Temperature and c) the PM$_1$ in the beginning of the corresponding experiment. The formed mass of ammonium nitrate in each experiment is also plotted (d) against the ambient gas phase ammonia in the beginning of the corresponding experiments.
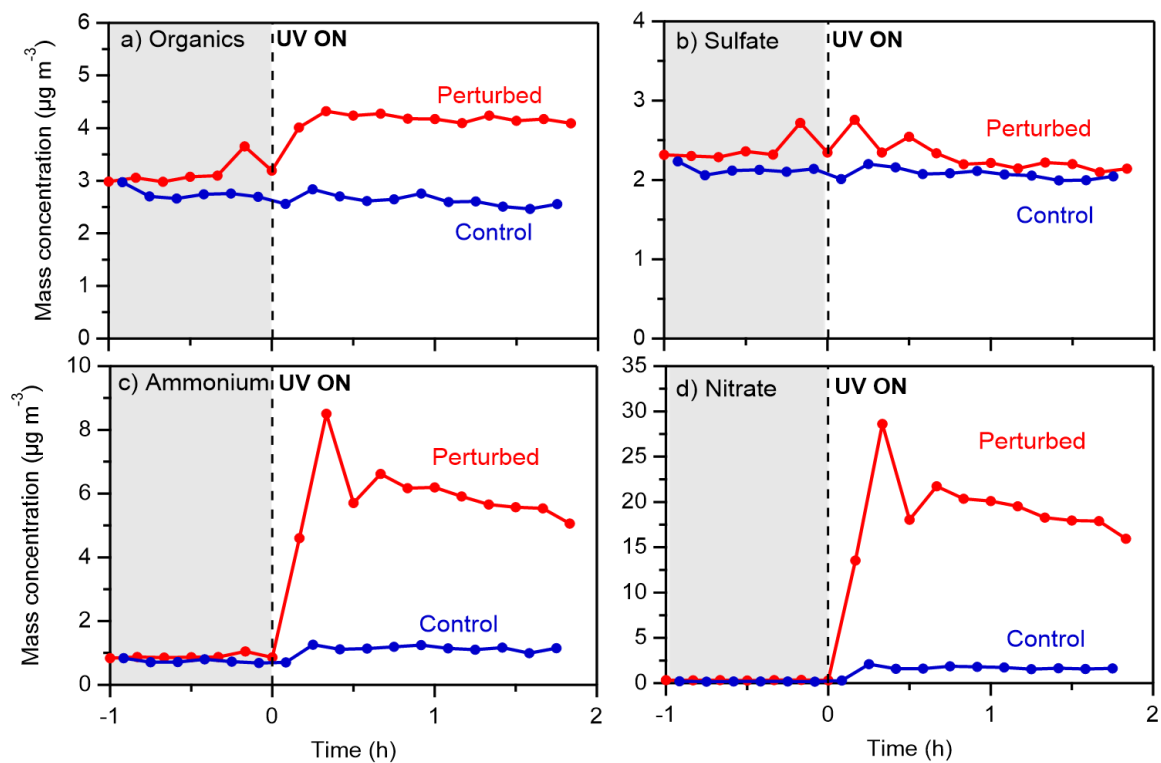
Figure 7: Wall-loss and CE corrected mass concentrations of a) organics, b) sulfate, c) ammonium and d) nitrate in the perturbed and the control chambers during Exp. 1 in Pertouli.
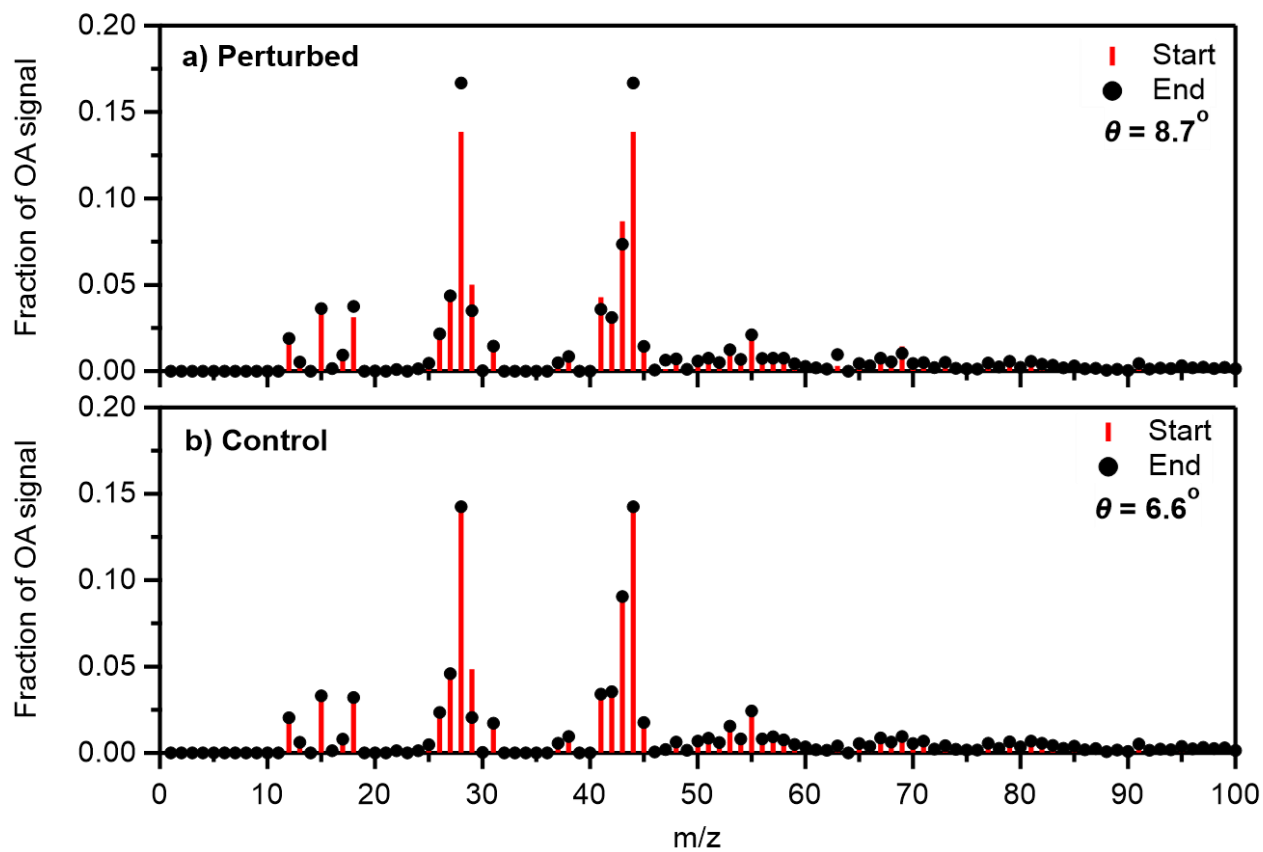
Figure 8: Average fractional signal of the organic aerosol at the start and the end of Exp. 1 in Pertouli in a) the perturbed and b) the control chambers.
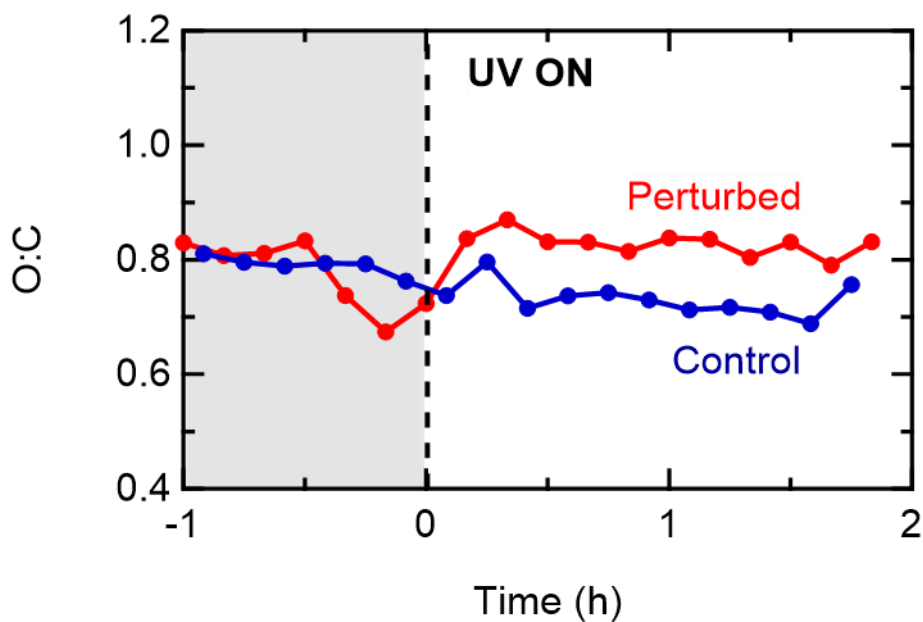
835 **Figure 9: Evolution of the O:C inside the perturbed and the control chambers during Exp. 1 in Pertouli.**
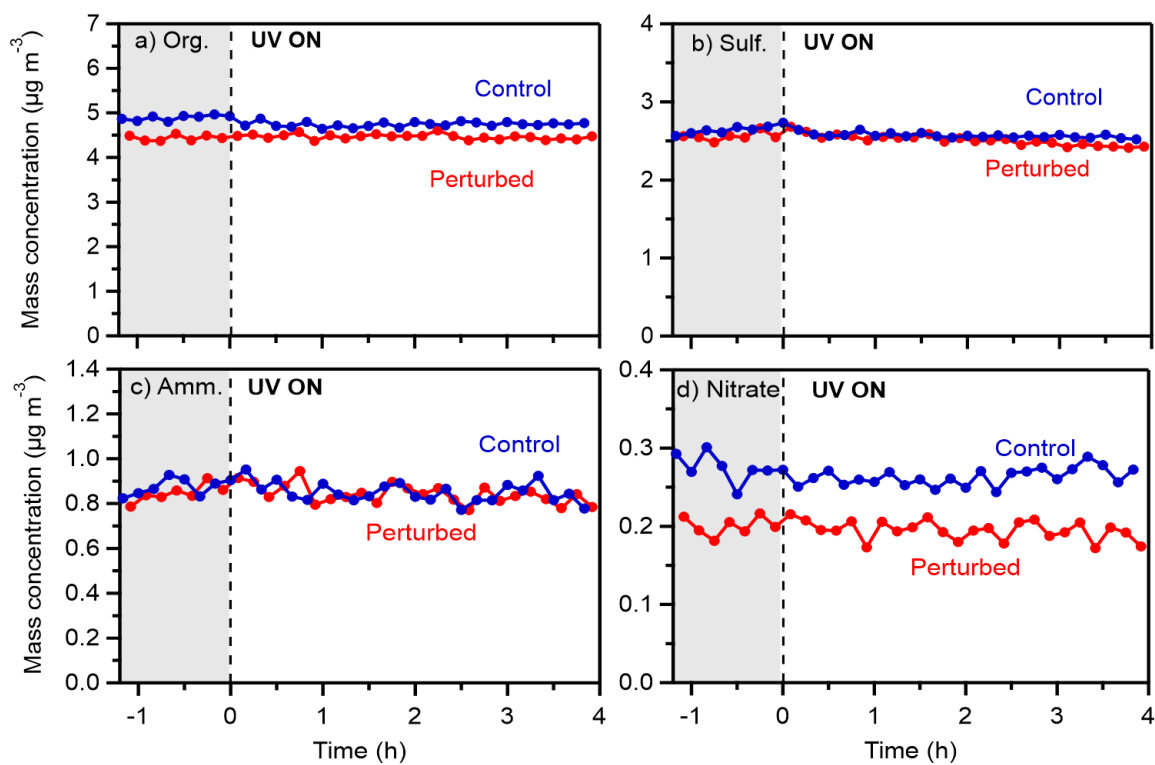
Figure 10: Wall loss corrected mass concentrations of a) organics, b) sulfate, c) ammonium and d) nitrate in the perturbed and the control chambers during Exp. 4 (20-7-2022) in Pertouli.